Accepted and Copyright: *Water Resources Research*
Article: Stewart, R. D., M. R. Abou Najm, D. E. Rupp, and J. S. Selker (2016), Modeling multidomain hydraulic properties of shrink-swell soils, *Water Resour. Res.*, *52*, doi:10.1002/2016WR019336.

Modeling multidomain hydraulic properties of shrink-swell soils

Ryan D. Stewart[1]*, Majdi R. Abou Najm[2], David E. Rupp[3], John S. Selker[4]

[1] *Crop and Soil Environmental Science Department, Virginia Polytechnic Institute and State University, Blacksburg, VA, United States.*

[2] *Civil & Environmental Engineering, American University of Beirut, Beirut, Lebanon*

[3] *Oregon Climate Change Research Institute, College of Earth, Ocean, and Atmospheric Sciences, Oregon State University, Corvallis, OR, United States.*

[4] *Biological & Ecological Engineering Department, Oregon State University, Corvallis, OR, United States.*

*Corresponding Author (ryan.stewart@vt.edu)

Abstract

Shrink-swell soils crack and become compacted as they dry, changing properties such as bulk density and hydraulic conductivity. Multidomain models divide soil into independent realms that allow soil cracks to be incorporated into classical flow and transport models. Incongruously, most applications of multidomain models assume that the porosity distributions, bulk density, and effective saturated hydraulic conductivity of the soil are constant. This study builds on a recently derived soil shrinkage model to develop a new multi-domain, dual-permeability model that can accurately predict variations in soil hydraulic properties due to dynamic changes in crack size and connectivity. The model only requires estimates of soil gravimetric water content and a minimal set of parameters, all of which can be determined using laboratory and/or field measurements. We apply the model to eight clayey soils, and demonstrate its ability to quantify variations in volumetric water content (as can be determined during measurement of a soil water characteristic curve) and transient saturated hydraulic conductivity, K_s (as can be measured using infiltration tests). The proposed model is able to capture observed variations in K_s of one to more than two orders of magnitude. In contrast, other dual-permeability models assume that K_s is constant, resulting in the potential for large error when predicting water movement through shrink-swell soils. Overall, the multi-domain model presented here successfully quantifies fluctuations in the hydraulic properties of shrink-swell soil matrices, and are suitable for use in physical flow and transport models based on Darcy's Law, the Richards Equation, and the advection-dispersion equation.

Introduction

Many clay-rich soils (often classified as *Vertisols* or *vertic*-intergrades) swell when wetted and shrink as they dry. The physical properties, such as pore size distribution and transient saturated hydraulic conductivity (i.e., effective permeability) of these soils are variable, due to alterations of their porous structure in response to changes in soil water content [*Messing and Jarvis*, 1990; *Jabro*, 1996; *Kutílek*, 1996; *Das Gupta et al.*, 2006]. However, most infiltration and transport models assume these properties are constant, and thus may perform poorly across different initial and time-varying soil water conditions.

A number of models have been developed to describe infiltration into *vertic* soils. Many frameworks represent the complexity of pore structures through multi-region pore models [*Gwo et al.*, 1995; *Hutson and Wagenet*, 1995; *Simunek et al.*, 2003]. The most common are dual-domain models representing macropores (such as soil cracks) and the soil matrix as two separate components of the soil. One subset of these models divide the soil into two porosity domains where flow occurs only in the macropore (mobile) domain [*Chen and Wagenet*, 1992; *Gerke*, 2006; *Jarvis*, 2007]. The macropore water flow has then been modeled using the Richards [*Novák et al.*, 2002], Poiseuille [*Ahuja et al.*, 2000], Chezy-Manning [*Chen and Wagenet*, 1992], kinematic wave [*Greco*, 2002; *Larsbo et al.*, 2005; *Römkens and Prasad*, 2006], or Green-Ampt [*Davidson*, 1984] equations. However, the simplifying assumption that water does not move through the soil matrix is unrealistic for many situations, including flow through many structured clay soils.

To remedy this short-coming, a subset of multi-domain models, known as dual-permeability, were developed to describe flow through both the macropores and the soil matrix, typically using the Richards equation [*Peters and Klavetter*, 1988; *Gerke and van Genuchten*, 1993; *Castiglione*

61 *et al.*, 2003; *Larsbo and Jarvis*, 2003; *Gerke and Köhne*, 2004; *Coppola et al.*, 2012;
62 *Lassabatère et al.*, 2014]. The dual-permeability approach applies a weighting factor (β) that
63 defines the fractional volumes of the matrix and fracture domains, which in turn determines their
64 combined contribution to total hydraulic conductivity (saturated and unsaturated). For the most
65 part, these models consider the size and properties of the fracture and matrix domains to be
66 constant in both time and space. *Coppola et al.* [2012]; *Coppola et al.* [2015] allowed β and/or
67 the soil hydraulic properties (e.g., volumetric water content, hydraulic conductivity) to vary as a
68 function of soil shrinkage. However, the relationships proposed in those models lack physical
69 consistency, in that domain-specific hydraulic properties (e.g., hydraulic conductivity) remain
70 constant regardless of changes in porosity distribution (e.g., β). This disconnect between
71 hydraulic properties and swelling implies that if data is fit to the model, then swelling-dependent
72 crack-flow may inadvertently be adjusted to account for changes in the matrix properties.
73 Ultimately this increases the number of uncertain parameters that must be obtained for each
74 model application and limits the ability of such models to predict dynamic changes in hydraulic
75 properties and corresponding hydrological processes.
76 A handful of field studies have determined, based on surface and subsurface infiltration
77 measurements, that the non-equilibrium (i.e., transient) field-saturated hydraulic conductivity of
78 clayey soils can vary with soil water content [*Messing and Jarvis*, 1990; *Jabro*, 1996; *Lin et al.*,
79 1998]. Specifically, these studies found that the transient field-saturated hydraulic conductivity
80 (K_s) is highest when the soil is at low initial (antecedent) water content, likely because in dry
81 conditions shrinkage cracks can act as preferential flowpaths. As the initial water content of the
82 soil increases, shrinkage cracks begin to seal and K_s undergoes a corresponding decrease.

Therefore, such findings indicate that the transient saturated hydraulic conductivity of the soil varies depending on the dynamic structure and distribution of pores and cracks.

Building on a recently developed pedon-scale porosity model that incorporates shrink-swell dynamics of aggregates, cracks, and subsidence [*Stewart et al.*, 2016], we propose a unifying model for the hydraulic properties of shrink-swell soils that inherits the dual-permeability framework. This model uses a consistent physical basis to predict changes in both porosity distribution and hydraulic properties of the soil as a function of water content. We provide examples of how this model can be used to properly relate domain-specific hydraulic properties with those of the entire soil profile, interpret water retention experiments on shrinking soils, and predict field-saturated hydraulic conductivity of *vertic* soils based on their initial moisture state. Altogether, the model accurately reproduces variations in soil hydraulic parameters and captures fundamental system behaviors, while utilizing a minimal and physically realistic set of input parameters.

Theory

In this section we describe the porosity domains of shrink-swell soils using two frames of reference. The first (which we call the “unified porosity”) employs a fixed, macro-scale control volume, wherein the overall porosity distribution shifts between aggregates, cracks and/or subsidence as the soil wets and dries. This representation of porosity is needed to correctly and accurately predict overall changes in porosity due to swelling and shrinking. However, to allow working within the classic dual domain porosity/permeability frame of reference (which we call the “multi-domain porosity”), we also describe the crack and aggregate porosity domains as independent from one another, and provide the means to convert between these frames of

reference (Figure 1). We conclude by using these porosity definitions to predict water content and field-saturated hydraulic conductivity of the independent soil domains and also of the entire soil. Note that the unified porosity framework was the subject of a previous publication [*Stewart et al.*, 2016]; we briefly reiterate the main results here so as to lay the foundation to derive our new dual-permeability model.

Unified porosity

Starting from a volume that is large enough to contain multiple soil pedons (the three-dimensional structural units of soil), *Stewart et al.* [2016] divided the total porosity (ϕ_{max}) among three domains, with each representing a fraction of pore space contained within the entire control volume:

$$\phi_{max} = \phi_{aggr}(U) + \phi_{sub}(U) + \phi_{crack}(U) \quad (1)$$

where ϕ_{aggr} is the porosity of the aggregate domain, ϕ_{crack} is the porosity associated with any shrinkage cracks that are present, and ϕ_{sub} is the porosity associated with any vertical subsidence that the soil has experienced (from its maximum surface elevation/volume). U represents the normalized gravimetric water content of the aggregate domain; i.e., $U = u_{aggr}/u_{max}$, where u_{aggr} is the gravimetric water content (mass of water per mass of dry soil) of the aggregate domain and u_{max} is the maximum mass of water per mass of dry soil that the soil profile can accommodate at saturation. In this formulation, the total porosity (ϕ_{max}) is constant, while the porosity distribution varies as a function of U. Note that though water can exist in the crack domain, water will only affect the porosity distribution when it is absorbed by the soil aggregate (i.e., matrix) causing the soil aggregates to swell.

Stewart et al. [2016] described the porosities of all three domains as functions of U as:

$$\phi_{aggr}(U) = (\phi_{max} - \phi_{min})\left(\frac{p+1}{p+U^{-q}}\right) + \phi_{\min} \quad (2)$$

$$\phi_{sub}(U) = (1-(1-(\phi_{max} - \phi_{min}))^{1/\chi})\left(\frac{1-U^{q}}{1+pU^{q}}\right) \quad (3)$$

$$\phi_{crack}(U) = \left((\phi_{max} - \phi_{\min}) - 1 + (1-(\phi_{max} - \phi_{min}))^{1/\chi}\right)\left(\frac{1-U^{q}}{1+pU^{q}}\right) \quad (4)$$

where p and q are functional shape parameters, ϕ_{min} is the minimum porosity of the aggregate domain, and χ is the shrinkage geometry factor [*Bronswijk*, 1990], which can range from 1 (pure subsidence) to ∞ (pure cracking), with the typical assumption that $\chi = 3$ (isotropic shrinkage).

Multi-domain porosity

Dual-porosity approaches treat the crack and aggregate porosity domains as independent from one another [*Gerke and van Genuchten*, 1993]. In such models, the total volume of the control volume is divided into two domains and two pore systems. The porosity of each domain is calculated in proportion to the total volume of the corresponding domain (rather than relative to the fixed control volume that is used in Equations (1) through (4)). Thus, to differentiate the independent domain porosities (pore volume is divided by domain volume) from the total porosities (pore volume is divided by total volume, as defined in Equations (1) to (4)), the symbol ε is used for the independent domain porosities while ϕ is used with total porosities. With this distinction in mind (and by initially neglecting subsidence), we can describe the total porosity of the soil in terms of the domain-specific crack (ε_{crack}) and aggregate (ε_{aggr}) porosities, coupled using a volumetric weighing factor, β, as:

$$\phi_{max} = \beta\varepsilon_{crack} + (1-\beta)\varepsilon_{aggr} \quad (5)$$

149 with β bounded by (0,1). Note that ε_{crack} is defined as the volume of voids within the crack
150 domain ($V_{v,crack}$) divided by the total volume of the crack domain ($V_{t,crack}$), and ε_{aggr} is defined as
151 the volume of voids within the aggregate domain ($\underline{V_{v,aggr}}$) divided by the total volume of the
152 aggregates ($V_{t,aggr}$). Also note that in many classic multi-domain formulations, $V_{v,crack}$ and $V_{t,crack}$
153 can differ from each other due to presence of "filling material" within the cracks [*Tsang and*
154 *Tsang*, 1987; *Gerke and van Genuchten*, 1993].
155 Typically, Equation (5) is applied assuming that β and the domain porosities ε_{crack} and ε_{aggr} are
156 constants. *Coppola et al.* [2015] examined how β and domain porosities could vary in shrink-
157 swell soils, though those results were limited to the specific case that deformation occurs only in
158 the horizontal direction (i.e., subsidence is not included), and only allowed porosity and β to
159 jointly vary under limited conditions (e.g., by specifying that β has to be an exponential function
160 of water content). Here, by making a few specific assumptions and definitions, we modify
161 Equation (5) to include the effects of subsidence and to provide a physically-consistent definition
162 of how the porosity distributions and β vary as functions of soil water content.
163 In our approach, we first assume that the crack domain is completely composed of voids (i.e.,
164 $V_{v,crack} = V_{t,crack}$), and therefore that $\varepsilon_{crack} = 1$. This assumption simplifies the system without
165 impacting the physical abstraction of cracking behavior, though is contrary to earlier
166 conceptualizations in which the crack domain is defined as occurring between sets of parallel
167 plates, and any soil/media within that delineation is considered to be part of the crack domain
168 [*Tsang and Tsang*, 1987; *Gerke and van Genuchten*, 1993]. In this present approach we also
169 assume that the subsidence domain is comprised of a single void.
170 Second, we let β be the summation of subsidence and crack total porosities and represent it as
171 function of U:

$$\beta(U) = \phi_{sub}(U) + \phi_{crack}(U) \quad (6),$$

which allows us to preserve Equation (5) while utilizing a physically-consistent description of how β varies with shrinkage and swelling.

Note that $\beta(U)$ can be considered as the "extra-aggregate" porosity of the soil (i.e., the combination of soil cracks and subsidence), and can be predicted by adding Equations (3) and (4) as:

$$\beta(U) = (\phi_{max} - \phi_{min})\left(\frac{1-U^q}{1+pU^q}\right) \quad (7).$$

With the definitions that $\varepsilon_{crack} = 1$ and $\beta = \phi_{sub}(U) + \phi_{crack}(U)$, comparison of Equations (1) and (5) shows that $\phi_{aggr} = (1-\beta)\varepsilon_{aggr}$, where ϕ_{aggr}, ε_{aggr} and β are all functions of water content U. Then, by combining Equations (2), (5), (6), and (7), we can describe ε_{aggr} in terms of the unified porosity model as:

$$\varepsilon_{aggr}(U) = \frac{\phi_{aggr}(U)}{1-\beta(U)} = \left[(\phi_{max} - \phi_{min})\left(\frac{p+1}{p+U^{-q}}\right) + \phi_{min}\right] \Bigg/ \left[1 - (\phi_{max} - \phi_{min})\left(\frac{1-U^q}{1+pU^q}\right)\right] \quad (8).$$

Water content

The overall water content of the control volume (θ) can be described as:

$$\theta = \theta_{crack} + \theta_{aggr} + \theta_{sub} \quad (9)$$

where θ_{crack} is the volumetric water content of the crack domain relative to the total control volume ($V_{w,crack}/V_t$, where the subscript w refers to water), θ_{aggr} is the volumetric water content of the aggregate domain relative to the total control volume ($V_{w,aggr}/V_t$), and θ_{sub} is the volumetric

water content of the subsidence domain relative to the total control volume ($V_{w,sub}/V_t$). In the absence of free water on the soil surface ($\theta_{sub} = 0$), Equation (9) can be simplified to:

$$\theta = \theta_{crack} + \theta_{aggr} \quad (10).$$

Similar to porosity, the volumetric water content can be represented as part of the total volume of the medium (θ as per the definition above) or as part of its corresponding porosity domain in a multi-porosity model (referred to as ζ). In the multi-porosity model, the crack and aggregate volumetric water contents (ζ_{crack} and ζ_{aggr}, respectively) are defined as follows: $\zeta_{crack} = V_{w,crack}/V_{t,crack}$ and $\zeta_{aggr} = V_{w,aggr}/V_{t,aggr}$.

Thus, Equation (10) can also be written in terms of the independent domain contributions as:

$$\begin{aligned}\theta_{total} &= \theta_{crack} + \theta_{aggr} = \left(\frac{V_{t,crack}}{V_t}\right)\left(\frac{V_{w,crack}}{V_{t,crack}}\right) + \left(\frac{V_{t,aggr}}{V_t}\right)\left(\frac{V_{w,aggr}}{V_{t,aggr}}\right) \\ &= \phi_{crack}(U)\zeta_{crack} + (1-\beta(U))\zeta_{aggr}\end{aligned} \quad (11)$$

Using Equation (11), the water content of the independent aggregate domain can be found by:

$$\zeta_{aggr} = \frac{\theta_{aggr}}{1-\beta(U)} = \theta_{aggr} \Bigg/ \left[1 - (\phi_{max} - \phi_{min})\left(\frac{1-U^q}{1+pU^q}\right)\right] \quad (12).$$

When working in vertic soils, water content is often measured and reported in gravimetric terms (i.e., mass of water over mass of solids). Thus, we define ζ_{aggr} in terms of its gravimetric water content:

$$\zeta_{aggr} = \left[u_{aggr}\gamma_s(1-\phi_{max})\right] \Bigg/ \left[1 - (\phi_{max} - \phi_{min})\left(\frac{1-U^q}{1+pU^q}\right)\right] \quad (13)$$

where γ_s is the specific gravity of the solid phase (i.e., the solid density, ρ_s, divided by the density of the fluid, ρ_f). This conversion is useful e.g. when determining water retention curves in shrink-swell soils.

Hydraulic conductivity

The water flux density through the dual-pore domains is described as:

$$J_{crack} = Q_{crack} / A_{crack} \quad (14a)$$

$$J_{aggr} = Q_{aggr} / A_{aggr} \quad (14b)$$

where Q_{crack} and Q_{aggr} are the volumes of water flowing per unit time through unit areas A_{crack} and A_{aggr}, respectively. Note that J is the vertical flux density, $A_{crack} = V_{t,crack}/H_m$ and $A_{aggr} = V_{t,aggr}/H_m$, and H_m is the height of the matrix.

The total flux density through the soil is given by:

$$J = \frac{Q_{crack} + Q_{aggr}}{A_{crack} + A_{aggr}} \quad (15).$$

The ratios of crack area A_{crack} and aggregate area A_{aggr} to the total area ($A_{total} = A_{crack} + A_{aggr}$) can be described by:

$$\frac{A_{crack}}{A_{crack} + A_{aggr}} = \frac{V_{crack} / H_m}{(V_{crack} + V_{aggr}) / H_m} = \left(\frac{\phi_{crack}(U)}{1 - \phi_{sub}(U)} \right) \quad (16a)$$

$$\frac{A_{aggr}}{A_{crack} + A_{aggr}} = \frac{V_{aggr} / H_m}{(V_{crack} + V_{aggr}) / H_m} = \left(\frac{V_{total} - V_{crack} - V_{sub}}{V_{total} - V_{sub}} \right) = \left(\frac{1 - \beta(U)}{1 - \phi_{sub}(U)} \right) \quad (16b).$$

Note that Equation (16) does not explicitly account for any pore or crack tortuosity, but will be valid so long as tortuosity is either minor or similar in magnitude between the two domains.

By combining Equations (14) – (16), the total flux density can also be expressed as:

$$J = \left(\frac{\phi_{crack}(U)}{1 - \phi_{sub}(U)} \right) J_{crack} + \left(\frac{1 - \beta(U)}{1 - \phi_{sub}(U)} \right) J_{aggr} \quad (17).$$

In the case of no vertical subsidence ($\phi_{sub} = 0$), Equation (17) reduces to the classic dual-permeability result: $J = \beta J_{crack} + (1-\beta) J_{aggr}$.

The pore water velocities v_{crack} and v_{aggr} are described by:

$$v_{crack} = J_{crack} / \zeta_{crack} \tag{18a}$$

$$v_{aggr} = J_{aggr} / \zeta_{aggr} \tag{18b}.$$

We can obtain an expression for the hydraulic conductivity of the soil (K_s) via Darcy's Law, which relates J to K_s and the gradient in potential $\nabla\Psi$:

$$K_s \nabla\Psi = \left(\frac{\phi_{crack}(U)}{1-\phi_{sub}(U)} \right) K_{crack} \nabla\Psi_{crack} + \left(\frac{1-\beta(U)}{1-\phi_{sub}(U)} \right) K_{aggr} \nabla\Psi_{aggr} \tag{19}.$$

If the gradient in potential is similar through the two domains (i.e., $\nabla\Psi \approx \nabla\Psi_{crack} \approx \nabla\Psi_{aggr}$), Equation (19) simplifies to:

$$K_s = \left(\frac{\phi_{crack}(U)}{1-\phi_{sub}(U)} \right) K_{crack} + \left(\frac{1-\beta(U)}{1-\phi_{sub}(U)} \right) K_{aggr} \tag{20}.$$

The standard assumption for dual-permeability models is that K_{crack} and K_{aggr} are constants [*Castiglione et al.*, 2003; *Coppola et al.*, 2015]. However, the volume of water per unit time (Q) that can be transmitted through a pore for a given potential gradient varies non-linearly with the pore area. If, for example, we assume a rectangular pore geometry, the Poiseuille Equation predicts $Q \propto yw^3$, where y is the length of the pore and w is the width of the pore. The area of the pore is $A_{pore} = yw$, so therefore the water flux through the pore is $J \propto w^2$ (or $J \propto r^2$ in the case of a cylindrical pore). We note that this prediction is only rigorously valid for Reynolds numbers less than one, which can be momentarily violated in large open cracks fed by ample water.

We represent cracks as a series of soil pedons surrounded by border cracks with constant length L_j (Figure 2) and a constant depth of H_m, and we account for any crack tortuosity using the parameter τ_j. Note that an alternative crack geometry is presented in the Appendix.

The crack porosity (ϕ_{crack}) can be expressed as:

$$\phi_{crack}(U) = \frac{V_{v,crack}}{V_t} = \sum_{j=1}^{N} \frac{w_j L_j \tau_j H_m}{V_t} = \left(\left(\phi_{max} - \phi_{\min}\right) - 1 + \left(1 - \left(\phi_{max} - \phi_{min}\right)\right)^{1/\chi}\right)\left(\frac{1 - U^q}{1 + pU^q}\right) \quad (21)$$

where $V_{v,cracks}$ is the total volume of cracks within the soil block containing N cracks.

Evaluating Equation (21) at $U = 0$ (when we assume that the cracks are at their maximum widths $w_{j,max}$) gives us:

$$\phi_{crack,max} = \sum_{j=1}^{N} \frac{w_{j,max} L_j \tau_j H_m}{V_t} = \left(\left(\phi_{max} - \phi_{\min}\right) - 1 + \left(1 - \left(\phi_{max} - \phi_{min}\right)\right)^{1/\chi}\right) \quad (22).$$

Combining Equations (21) and (22), we obtain the result of *Stewart et al.* [2016]:

$$\sum_{j=1}^{N} w_j = \sum_{j=1}^{N} w_{j,\max}\left(\frac{1 - U^q}{1 + pU^q}\right) \quad (23a)$$

which, so long as the cracks all change width in proportion to one another, simplifies to:

$$w_j = w_{j,\max}\left(\frac{1 - U^q}{1 + pU^q}\right) \quad (23b).$$

Assuming that the cracks maintain consistent geometries, we can use the Poiseuille equation to approximate the hydraulic conductivity of the crack domain as:

$$K_{crack}(U) = \sum_{j=1}^{N} \frac{A_j \rho_f g w_j^{\,2}}{12\mu_f A_{crack} \tau_j^{\,2}} = \sum_{j=1}^{N} \frac{L_j \rho_f g w_j^{\,3}}{12\mu_f \sum_{j=1}^{N} L_j w_j \tau_j^{\,2}} \quad (24)$$

where A_j is the cross-sectional area of crack j, A_{crack} is the total cross-sectional area of all cracks, ρ_f is the density of the fluid (water), g is the gravitational acceleration, and μ_f is the fluid viscosity. Substituting Equation (23) into (24), we obtain:

$$K_{crack}(U) = \sum_{j=1}^{N} \frac{L_j \rho_f g w_{j,max}{}^3 \left(\frac{1-U^q}{1+pU^q} \right)^3}{12\mu_f \sum_{j=1}^{N} L_j \tau_j{}^2 w_{j,max} \left(\frac{1-U^q}{1+pU^q} \right)} = K_{crack,max} \left(\frac{1-U^q}{1+pU^q} \right)^2 \quad (25a)$$

$$K_{crack,max}(U) = \sum_{j=1}^{N} \frac{L_j \rho_f g w_{j,max}{}^3}{12\mu_f \sum_{j=1}^{N} L_j \tau_j{}^2 w_{j,max}} \quad (25b)$$

where $K_{crack,max}$ is the maximum hydraulic conductivity of the crack domain (when $U = 0$). We can do a similar treatment for the aggregate domain. So long as the subsidence is minor relative to the overall height of the soil block and all soil pores shrink-swell in proportion to one another, we can predict the radius of any aggregate pore, r_i, as [*Stewart et al.*, 2016]:

$$r_i{}^2 = \left(r_{i,\max}{}^2 - r_{i,\min}{}^2 \right) \left(\frac{p+1}{p+U^{-q}} \right) + r_{i,\min}{}^2 \quad (26).$$

If we assume that the aggregate domain is composed of a number M of vertical cylindrical pores that vary in proportion to one another, we can use the Poiseuille equation to calculate the hydraulic conductivity of that domain (K_{aggr}) as:

$$K_{aggr}(U) = \sum_{i=1}^{M} \frac{A_i \rho_f g r_i{}^2}{8\mu_f A_{aggr} \tau_i{}^2} \quad (27)$$

where τ_i is the tortuosity factor for pore i and A_i is the area of pore i (in this case assumed to be equal to πr_i^2). So long as the pores all change size in proportion to one another during

shrinkage/swelling, the ratio of $A_i/A_{aggr} = A_{i,max}/A_t = \pi r_{i,max}^2/A_t$. We can then obtain K_{aggr} in terms of U by substituting Equation (26) into Equation (27):

$$K_{aggr}(U) = \sum_{i=1}^{M} \frac{\pi r_{i,max}^{\ 2} \rho_f g}{8\mu_f A_t \tau_i^{\ 2}} \left(\left(r_{i,max}^{\ 2} - r_{i,min}^{\ 2} \right) \left(\frac{p+1}{p+U^{-q}} \right) + r_{i,min}^{\ 2} \right) \quad (28).$$

We can rearrange Equation (28) as:

$$K_{aggr}(U) = \sum_{i=1}^{M} \sqrt{\frac{\pi r_{i,max}^{\ 2} \rho_f g}{8\mu_f A_t \tau_i^{\ 2}}} r_{i,max}^{\ 2} \left(\frac{p+1}{p+U^{-q}} \right) + \sum_{i=1}^{M} \sqrt{\frac{\pi r_{i,max}^{\ 2} \rho_f g}{8\mu_f A_t \tau_i^{\ 2}}} r_{i,min}^{\ 2} \left(\frac{1-U^q}{1+pU^q} \right) \quad (29).$$

Solving Equation (29) for $U = 0$ and $U = 1$ gives us:

$$K_{aggr}(U=0) = K_{aggr,min} = \sum_{i=1}^{M} \frac{\pi r_{i,max}^{\ 2} \rho_f g}{8\mu_f A_t \tau_i^{\ 2}} r_{i,min}^{\ 2} \quad (30a)$$

$$K_{aggr}(U=1) = K_{aggr,max} = \sum_{i=1}^{M} \frac{\pi r_{i,max}^{\ 2} \rho_f g}{8\mu_f A_t \tau_i^{\ 2}} r_{i,max}^{\ 2} \quad (30b).$$

Substituting Equation (30) into Equation (29), we obtain:

$$K_{aggr}(U) = K_{aggr,max} \left(\frac{p+1}{p+U^{-q}} \right) + K_{aggr,min} \left(\frac{1-U^q}{1+pU^q} \right) \quad (31).$$

Further, if $K_{aggr,min} << K_{aggr,max}$, Equation (31) simplifies to:

$$K_{aggr}(U) = K_{aggr,max} \left(\frac{p+1}{p+U^{-q}} \right) \quad (32).$$

Substituting Equations (25) and (32) into Equation (17) and applying Darcy's Law for a similar gradient in potential (i.e., $\nabla\Psi \approx \nabla\Psi_{crack} \approx \nabla\Psi_{aggr}$) allows us to describe the saturated transient hydraulic conductivity K_s of the bulk soil as:

294 $$K_s = K_{crack,max}\left(\frac{\phi_{crack}(U)}{1-\phi_{sub}(U)}\right)\left(\frac{1-U^q}{1+pU^q}\right)^2 + K_{aggr,max}\left(\frac{1-\beta(U)}{1-\phi_{sub}(U)}\right)\left(\frac{p+1}{p+U^{-q}}\right) \quad (33).$$

295

296 **Methods**

297 *Study sites*

298 As part of this study, single ring infiltration measurements were performed at two sites. The first
299 was located in western Oregon, within a 2 m x 3 m area in a field located near Corvallis, Oregon.
300 The soil in the area is classified as a Waldo silty clay loam, a *fine, smectitic, mesic Fluvaquentic*
301 *Vertic Endoaquoll* with moderate to high shrink-swell potential [*Knezevich,* 1975]. Hydrometer
302 measurements on soil samples we collected detected 5% sand, 37% silt and 58% clay, giving it a
303 clay texture.
304 In this site, single ring infiltration tests were conducted monthly over the following timespans:
305 September 2011 – December 2011; February 2012 – May 2012; October 2012 – March 2013 (13
306 sampling events in total). On each testing date, twelve infiltration measurements were collected
307 using a spatially distributed array of twelve 9.6 cm diameter rings. Each ring was inserted into
308 the soil to a depth of approximately 1 cm. The rings were left in the same place for the first year
309 (September 2011 – May 2012). On all dates after October 2012 the rings were randomly
310 positioned before testing.
311 The second site was located in south-central Chile, in a set of 3.5 x 11 m instrumented plots
312 located near the community of Ninhue. The soil is classified as a Cauquenes-series clayey soil.
313 Hydrometer measurements showed that the near-surface (0-20 cm) soil had 44% sand, 31% silt,
314 and 25% clay, giving it a loam texture. 158 infiltration tests were performed over a three-week
315 period in January 2012, when the plots received heavy irrigation and transitioned from very dry

316 to near-saturated conditions (gravimetric water contents increased from 0.05 to 0.46, as
317 measured from duplicate cores collected from the site at times of testing). For more details on the
318 experimental site, see *Stewart et al.* [2015]; details on shrinkage and swelling measurements for
319 these soils are found in *Stewart et al.* [2012] and *Stewart et al.* [2016].
320
321 *Infiltration testing procedure*
322 For each infiltration test, water was added to the ring in 0.1 L increments (equivalent to 1.38 cm
323 depth), which allowed for slightly positive constant head conditions ($h \geq 0$) to be approximated
324 [*Haverkamp et al.*, 1998; *Braud et al.*, 2005; *Bagarello et al.*, 2014]. Each increment of water
325 was added to the ring once the water level had fallen enough to expose approximately 50% of the
326 soil surface, and the elapsed time was recorded. Up to 1 L (13.8 cm) of water in total was added.
327 As part of each infiltration test, soil samples were collected from two depths – 8 cm and 12 cm –
328 at three random locations within the plot. The soil samples were 5.4 cm in diameter and 3 cm in
329 length, for a total volume of 69 cm^3, and were used to determine the initial bulk density,
330 gravimetric water content, and porosity at the time of testing.
331 Seven and 17 soil cores from the Oregon and Chile sites, respectively, were placed into 5.7 cm
332 diameter by 3 cm long Tempe cells and analyzed for their saturated hydraulic conductivity (K_s)
333 using either the constant head method (for the more permeable samples) or the falling head
334 method (for the less permeable samples) [*Klute and Dirksen*, 1986]. One sample was also tested
335 using a modified flexible wall permeameter. The measured K_s values were of the same order of
336 magnitude using either method; therefore, the rigid Tempe cell measurements were considered
337 adequate to estimate K_s.
338

Data Analysis

The infiltration test data were analyzed using the two-term Philip infiltration model rewritten in the general form suggested by *Smiles and Knight* [1976]:

$$\frac{I}{t^{1/2}} = S + Ct^{1/2} \tag{34}$$

where I is the cumulative infiltration [L], t is the elapsed time [T], S is the soil sorptivity, and C is a constant that accounts for gravity effects (for one-dimensional vertical infiltration) or combined gravity and capillarity effects (in the case of three-dimensional infiltration). Using Equation (34), C can be determined as the slope of a line fit to infiltration data (e.g., Figure 3, which shows an example data set collected from the Oregon site in May).

Next, using the three-dimensional infiltration (I_{3D}) model developed by *Wu et al.* [1999], we assumed that the C term is equal to:

$$C = afK_s \tag{35}$$

where a is a constant assumed to be equal to 0.9 and K_s is the saturated hydraulic conductivity of the soil. Following *Wu et al.* [1999], the parameter f for slightly-ponded (h = 0) conditions is taken to be:

$$f = \frac{\Lambda / K_s}{d + r_d / 2} + 1 \tag{36}$$

where Λ is the matrix flux potential of the soil (related to soil texture and antecedent conditions), d is the depth of ring insertion and r_d is the radius of the ring. Λ/K_s was assumed to be 25 cm, based on the van Genuchten parameters fit to water retention measurements collected on 34 soil cores (28 from the Chile site, six from the Oregon site) and the capillary drive model proposed by *Morel-Seytoux et al.* [1996]. Note that the individual estimates of Λ/K_s ranged from 2 to 55

cm for the Oregon soil (standard error of the mean = 8.6 cm) and from 5 to 120 cm for the Chile soil (standard error of the mean = 4.3 cm).

Other Studies

To verify that the proposed relationships are applicable to a wider range of soils, we compiled published results from five studies that examined variability in porosity, water content, and/or transient hydraulic conductivity due to shrinkage and swelling:

1. *Horn et al.* [2014] analyzed a Haplic Stagnosol (German) soil (65% clay content) for relationships between water content (as moisture ratio) and porosity (as void ratio) and between volumetric water content and matric potential (ψ), with and without accounting for shrinkage.

2. *Corbeels et al.* [1999] studied the use of a neutron moisture meter in a Chromic Calcixerert soil in Morocco. As part of the study, the authors collected aggregate-scale bulk density measurements ($\rho_{b,aggr}$) using soil cores and clods across a range of gravimetric water contents. We converted these bulk density values to the domain-dependent aggregate porosity by assuming that $\varepsilon_{aggr} = 1 - \rho_{b,aggr}/\rho_s$, with the solid density given as $\rho_s = 2.7$ Mg m^{-3}. We also determined the domain-dependent aggregate water content as $\zeta_{aggr} = u * \rho_{b,aggr}/\rho_w$, where ρ_w is the density of water (1.0 Mg m^{-3}).

3. *Messing and Jarvis* [1990] measured soil shrinkage curves and seasonal variability of field-saturated hydraulic conductivity (using borehole infiltration tests) at two sites in Sweden: Limsta, where the soils are 65-80% clay, and Ultana, where the soils are 45-60% clay.

4. *Jabro* [1996] measured transient saturated hydraulic conductivity every month for 1.5 yr using a Guelph permeameter. This study was done in a Hagerstown (Pennsylvania) soil, a mixed-mineralogy silt loam with typical COLE values of 0.02-0.04.

5. *Lin et al.* [1998] made surface infiltration measurements using a tension infiltrometer for seven different vertic soils in Texas. We focus on their infiltration measurements collected in a river bottomland Vertisol (Ships series soil) under ponded (h = 0 cm) conditions. Note that only steady-state infiltration rates were presented, so we assumed that these infiltration values were proportional to the field-saturated hydraulic conductivity, and thereby we scaled all observations relative to the maximum, i.e., assuming $i/i_{max} = K_s/K_{s,max}$.

Model Fitting

For the datasets with measured soil shrinkage curves (i.e., the Waldo silty clay (Oregon) loam, Cauquenes (Chile) loam, Ultana and Limsta (Sweden) clays, Haplic Spagnosol (German) clay, and Chromic Calcixerert (Morocco) clay), unless reported directly, ϕ_{min}, ϕ_{tot} and u_{max} were estimated from the endpoint values of their corresponding figures and graphs. We constrained ϕ_{max} and u_{max} by $u_{\max} = \rho_f \phi_{max} / \rho_s (1 - \phi_{max})$, where ρ_f is the fluid density (assumed here to be 1.0 g cm^{-3}) and ρ_s is the density of solids (assumed here to be 2.7 g cm^{-3}). The soil shrinkage curve parameters p and q were found by fitting Equation (2) (or Equation (9), in the case of the Morocco soil) to the observed data with the default nonlinear least squares (NLS) algorithm within *R*. For the Haplic Spagnosol (German) clay soil, the NLS fitting algorithm was used to fit the van Genuchten water retention function, which predicts volumetric water content θ as a function of matric potential ψ as $\theta = (\theta_s - \theta_r)\left(1 + (\alpha\psi)^n\right)^{-m} + \theta_r$, by adjusting the parameters θ_r, α, and n. θ_s was assumed to be equal to ϕ_{max}.

Next, the NLS algorithm was used to solve for $K_{crack,max}$ and $K_{aggr,max}$ in Equation (33) using the observed transient hydraulic conductivity (K_s) as the target. Note that the final two soils – Hagerstown (Pennsylvania) silty loam and Ships (Texas) clay – did not include soil shrinkage

406 measurements. In these cases, ϕ_{max} and u_{max} were found using the maximum reported water
407 contents while ϕ_{min} was treated as a fitting parameter. The NLS algorithm was used in
408 combination with Equation (33) and the observed K_s values to determine p, q, $K_{crack,max}$, and
409 $K_{aggr,max}$. Isotopic shrinkage (i.e., the shrinkage geometry factor $\chi = 3$) was assumed for all soils.
410

411 **Results and Discussion**

412 The set of multi-domain models presented here require eight parameters in total: p, q, ϕ_{max}, ϕ_{min},
413 u_{max}, χ, $K_{crack,max}$, and $K_{aggr,max}$. Aggregate-scale soil shrinkage measurements, such as the
414 generation of soil shrinkage curves (e.g., Figure 4a, Figure 5a), can be used to estimate the
415 parameters p, q, ϕ_{max}, ϕ_{min}, and u_{max}. As an example, Figure 4a shows the measured porosity of
416 the Haplic Stagnosol (German) soil as a function of decreasing soil water content (points), fit
417 using Equation (2) (solid line; final parameter values are listed in Table 1). Once the soil
418 shrinkage parameters (i.e., p, q, ϕ_{max}, ϕ_{min}, and u_{max}) were determined, Equation (7) was used to
419 evaluate the weighting function β (dotted line) and Equation (8) was used to determine the
420 domain-specific aggregate porosity ε_{aggr} (dashed line). These porosity domain descriptions can
421 then be used to accurately interpret water content and water retention relationships (Figure 4b).
422 In this example, water content and soil suction were measured for the Haplic Stagnosol soil. The
423 water retention behavior of the aggregates can then be described either in terms of the overall
424 volumetric water content (θ_{aggr}) or the domain-specific volumetric water content (ζ_{aggr}), with the
425 $\beta(U)$ function (again estimated by Equation (7)) serving as an accurate means by which to
426 convert the two. Thus, Equations (2) – (8) represent a physically-consistent and tractable (i.e.,
427 can be parameterized from relatively simple laboratory measurements) means of determining the
428 dynamic porosity domain functions.

These relationships between porosity domains can also be used when calibrating *in situ* measurements of soil water content, e.g., with a thermal neutron probe. Using aggregate-scale bulk density data from *Corbeels et al.* [1999] for the Chromic Calcixerert (Morocco) soil, we determined the soil shrinkage curve for field conditions (Figure 5a). We then used the relationships of Equation (13) to create a constitutive relationship between gravimetric and volumetric water contents (Figure 5b), similar to the result obtained by the authors in their original analysis. Because most moisture-sensing technologies report water content in terms of volumetric water content, such analyses can be useful when working in shrink-swell soils.

The soil shrinkage curve was also used to determine model parameters for the Waldo silty clay loam (Oregon) soil (Figure 6a), the Cauquenes (Chile) soil (Figure 7a), and the two Swedish soils (Figure 8a). In these cases, the parameters u_{max}, ϕ_{max}, ϕ_{min}, p, and q were readily found by fitting Equation (2) to the observed data. This procedure then reduces to two the number of uncertain parameters ($K_{crack,max}$, $K_{aggr,max}$) required to describe variations in field-saturated hydraulic conductivity (K_s) due to shrinkage and swelling (i.e., using Equation (33)). In the case of these four soils, Equation (33) provides a reasonable fit to the observed variations in K_s (Figures 6b; 7b; 8b), with coefficient of determination (r^2) values above 0.6 for three of the four soils. The Ultana (Swedish) clay soil had an r^2 value of only 0.1, likely caused by the relatively few number of observations (eight points in total, and none at a low crack porosity) and the presence of a single K_s value that is one to two orders of magnitude higher than the other measurements done at a similar crack porosity. This outlier point could be explained by heterogeneity in crack structures within the various boreholes or perhaps could be due to hysteresis between shrinking and swelling phases (either of which are beyond the capability of this model). This particular site also did not include any observations at high water contents/low

crack porosities, which resulted in a relatively high estimate for $K_{aggr,max}$ compared to other sites. If we instead combine the two Swedish soils together before performing the regression (as the authors did in the original study), the coefficient of determination increases to $r^2 = 0.73$ (indicated by the dashed line in Figure 8b).

K_s values for the Hagerstown (Pennsylvania) silt loam (Figure 9) and the Ships (Texas) clay (Figure 10) were also modeled with Equation (33). In these locations, however, independent soil shrinkage measurements as a function of water content were not reported. Thus, to fit Equation (33) to these observations, we needed to optimize four parameters ($K_{crack,max}$, $K_{aggr,max}$, p, q). This had the benefit of improving the model fits relative to the previous examples, as both of these soils had r^2 values above 0.9. However, this approach increased parameter uncertainty (due to fitting more parameters from the same basic measurements) and in general may require more observations (e.g., infiltration measurements across a range of water contents) in order to satisfactorily parameterize the model compared to instances where soil shrinkage curves are available.

Here we note that for most of these examples, Equation (33) predicts that the lowest K_s value will occur at moderate water contents (rather than at $U = 1$, as might be expected). This effect may be more prominent in soils that have small differences between the predicted $K_{crack,max}$ and $K_{aggr,max}$ values. As an example, the Cauquenes (Chile) soil had relatively minor variation in K_s values between wet and dry conditions (approximately 1 – 1.5 orders of magnitude). As a result, Equation (33) predicted that the minimum K_s value (5.7 mm hr^{-1}) will occur at approximately $U = 0.6$, whereas the infiltration tests showed that the minimum mean K_s value occurred at $U = 0.9$. While there may be instances where this effect has a physical basis, considering that at moderate water contents the aggregate pores may have partially sealed while the shrinkage cracks may be

475 under-developed and not well-connected, no evidence of a minimum K_s occurring at $U < 1$ is
476 apparent in any of the data analyzed here. This effect can also be reduced by including the
477 $K_{aggr,min}$ term (e.g., as shown in Equation (31)), though in our analysis the slight model
478 improvement that may be gained by including this parameter does not outweigh the increased
479 model uncertainty. Note that including the $K_{aggr,min}$ term also allows aggregate pores to possess
480 non-zero hydraulic conductivity in dry conditions, and so future model refinements may explore
481 this term in more detail.
482 Laboratory-based K_s measurements were also performed using soil cores collect from the Waldo
483 silty clay loam (Oregon) and Cauquenes loam (Chile) soils. Our hypothesis was that these
484 samples, when collected in wet conditions ($U > 0.5$) and analyzed in saturated conditions ($U = 1$)
485 would represent the hydraulic conductivity of the aggregate domain (i.e., $K_{aggr,max}$). The
486 Cauquenes soil cores ($n = 18$) had a geometric mean K_s values of 4.7 mm hr^{-1}. This is within a
487 factor of two of the $K_{aggr,max}$ value determined using the field infiltration measurements ($K_{aggr,max}$
488 = 6.9 mm hr^{-1}), and is also close to the mean K_s value observed in the field when $U = 0.89$ (K_s =
489 3.2 mm hr^{-1}). However, the Waldo (Oregon) soil cores ($n = 7$) had a geometric mean of $K_s = 270$
490 mm hr^{-1}, whereas the $K_{aggr,max}$ value determined from field infiltration measurements was
491 predicted to be 3.4 mm hr^{-1}. One possible reason for the discrepancy between the two soils was
492 that samples from the Waldo soil came exclusively from near the surface, at depths of 5 – 15 cm.
493 When dealing with any soil core, but in particular well-structured surface soils, it is common to
494 find that laboratory K_s measurements show much higher values compared to field settings
495 [*Bouma*, 1980; *Reynolds et al.*, 2000]. The Cauquenes soil cores, on the other hand, came from
496 both the surface and the subsurface, including samples collected at 30, 60 and 75 cm depths.
497 These deeper samples in general had higher proportion of swelling 2:1 clays and showed K_s

values that were overall 1-2 orders of magnitude less than the K_s values of the near-surface samples. On the whole, these results suggest that field infiltration measurements are likely more instructive overall when assessing the hydraulic conductivity of shrink-swell soils, yet there may be some predictive value in aggregate-scale core samples.

Finally, we note that as cracks exceed some critical width, inertial forces and local accelerations will become important and water flowing through the crack will become fully turbulent. In these situations, the flow will begin to depart from Darcy's law, and the effective (transient) saturated hydraulic conductivity will become smaller than that predicted from the actual crack widths. As such, the cracks widths used for example in Equation (25) may represent effective rather than true widths. While previous experimental work has shown the assumption of laminar Poiseuille flow to be adequate for predicting K_s even with macropores ~0.5 cm in diameter [*Dunn and Phillips*, 1991], wide cracks (i.e., >> 1 mm) may require hydrodynamic or kinetic equations (e.g., Lattice Boltzmann methods, [*Sukop et al.*, 2013]) in order to accurately relate true crack widths with observed flow patterns. Nonetheless, given the reasonably good fits between observed and theoretical hydraulic conductivities for the different soils included in this analysis, we are confident that model developed here is applicable to many shrink-swell soils. Moreover, the multi-domain relationships between porosity and crack width used here to define K_s should be adaptable for use during film flow conditions (e.g., *Nimmo* [2010; 2016]) and/or with discretized vertical schemes (e.g., VIMAC; *Greco* [2002]), thereby in the future allowing processes such as non-uniform adsorption and swelling to be modeled.

Conclusions

520 We proposed a unified modeling framework for shrink-swell soils, in which the dynamic
521 distribution of soil porosity is described in terms of three distinct domains (aggregates, cracks,
522 subsidence). This framework varies from previous models by allowing for variations in the
523 hydraulic properties (e.g., saturated hydraulic conductivity) of the aggregate and crack domains
524 (whereas previous models assumed that such properties are constant), and by incorporating
525 subsidence. Within the new framework, we are able to consistently predict the dual-domain
526 weighting factor, $\beta(U)$, which, it should be noted, is another traditional source of uncertainty
527 when applying dual-permeability concepts to shrink-swell soils. We then use this weighting
528 function to relate the hydraulic properties of the individual domains to that of the overall soil.
529 This effort culminates in a new expression to describe transient saturated hydraulic conductivity
530 (K_s) as a dynamic property that varies as a function of soil water content. As a result, we are able
531 to predict variation in hydraulic conductivity in time for a given location.
532 Based on the observations from these six soils, the new K_s equation is able to describe 10 to 99%
533 of the observed variation in K_s (as quantified using the coefficient of determination, r^2; Table 1),
534 with all but one soil above $r^2 = 0.6$. The new K_s model requires eight parameters in total (ϕ_{max},
535 ϕ_{min}, χ, u_{max}, $K_{crack,max}$, $K_{aggr,max}$, p, and q); however, the maximum porosity ϕ_{max} and the
536 maximum gravimetric water content u_{max} can be related given estimates of the soil solid phase
537 density and the fluid density, reducing the number of unknown parameters by one. Moreover,
538 five of these parameters (ϕ_{max}, ϕ_{min}, u_{max}, p, and q) can be estimated from laboratory-scale
539 measurements of soil shrinkage properties, and a sixth (χ) can be constrained if the shrinkage
540 geometry factor is known or estimated. This leaves just two parameters that need to be estimated
541 from infiltration tests ($K_{crack,max}$, $K_{aggr,max}$). While in most instances these parameters are likely
542 best estimated in the field, we performed some preliminary analyses examining the relationship

of these parameters with K_s values measured in rigid and flexible-wall permeameters. In one instance, the laboratory cores gave estimates of K_s that were closely related with the hydraulic conductivity values measured in the field during wet antecedent conditions. In the other location, however, the laboratory measurements showed K_s values that were nearly two orders of magnitude greater than those observed in the field under wet conditions and on the same order of magnitude as those observed in the field under dry conditions. Therefore, while there may be some predictive value in small-scale laboratory measurements of the aggregate domain hydraulic conductivity, this result requires further investigation. We also note here that the relationships developed in this analysis are focused solely on saturated water movement and that there still remain gaps in understanding of how unsaturated hydraulic conductivity evolves during shrinkage and swelling processes.

The dual-domain model presented here represents a successful attempt to simulate how porosity changes cause dynamic variations in the hydraulic properties of shrink-swell soil matrices, while maintaining parsimony in the number and type of required parameters. As such, in many instances the model can be used with physical flow and transport models based on Darcy's Law, the Richards Equation, and the advection-dispersion equation. At the same time, the domain-specific definitions of crack and aggregate water contents are needed to satisfactorily convert between volumetric and gravimetric water contents, for example when measuring water content with neutron probe or capacitance-based sensors. Altogether, due to reduced uncertainty and more realistic hydraulic descriptions, this model will improve understanding and prediction of non-equilibrium flow and transport processes.

Appendix – Alternative geometric description of soil cracks

Here we modify our result for soils characterized by small cracks that are contained within the soil blocks rather than surrounding them. We assume in this case that each individual crack has some length y_j and width w_j that vary proportionally to one another, and that each crack has a constant depth of z_j, where $z_j \leq H_m$ (H_m being the total height of the matrix at any given water content, u_{aggr}).

The crack porosity (ϕ_{crack}) can be expressed as:

$$\phi_{crack}(U) = \frac{V_{v,crack}}{V_t} = \sum_{j=1}^{N} \frac{w_j y_j z_j}{V_t} = \left(\left(\phi_{max} - \phi_{\min}\right) - 1 + \left(1 - \left(\phi_{max} - \phi_{min}\right)\right)^{1/\chi}\right)\left(\frac{1 - U^q}{1 + pU^q}\right) \quad \text{(A1)}$$

where $V_{v,cracks}$ is the total volume of cracks within the soil block containing N cracks.

Evaluating Equation (A1) at $U = 0$ (when we assume that the cracks are at their maximum widths $w_{j,max}$ and lengths $y_{j,max}$) gives us:

$$\phi_{crack,max} = \sum_{j=1}^{N} \frac{w_{j,max} y_{j,max} z_j}{V_t} = \left(\left(\phi_{max} - \phi_{\min}\right) - 1 + \left(1 - \left(\phi_{max} - \phi_{min}\right)\right)^{1/\chi}\right) \quad \text{(A2).}$$

If we assume that the cracks maintain a consistent geometric proportionality (e.g., $w_j / w_{j,max} = y_j / y_{j,max}$; $w_j / w_{j+1} = w_{j,max} / w_{j+1,max}$), we can combine Equations (A1) and (A2) as:

$$\sum_{j=1}^{N} w_j^{\,2} = \sum_{j=1}^{N} w_{j,\max}^{\,2}\left(\frac{1 - U^q}{1 + pU^q}\right) \quad \text{(A3a)}$$

$$w_j^{\,2} = w_{j,\max}^{\,2}\left(\frac{1 - U^q}{1 + pU^q}\right) \quad \text{(A3b).}$$

The Poiseuille equation can be used to approximate the hydraulic conductivity of the crack domain as:

$$K_{crack}(U) = \sum_{j=1}^{N} \frac{A_j \rho_f g w_j^{\,2}}{12 \mu_f A_{crack}} \quad \text{(A4)}$$

where A_j is the cross-sectional area of crack j, γ_f is the specific density of the fluid (water), and μ_f is the fluid viscosity. So long as the cracks maintain proportional geometries to one another, $A_j/A_{crack} = A_{j,max}/A_{crack,max}$ and we can treat those terms as constants. By taking the ratio of Equation (A4) relative to its maximum value (when $U = 0$) and using the relationship of Equation (A3), we obtain:

$$\frac{K_{crack}(U)}{K_{crack,max}} = \frac{\sum_{j=1}^{N} w_j^{\,2}}{\sum_{j=1}^{N} w_{j,max}^{\,2}} = \left(\frac{1-U^q}{1+pU^q}\right) \tag{A5}$$

where $K_{crack,max}$ is the maximum hydraulic conductivity of the crack domain (when $U = 0$). Combining Equations (A4) with Equations (17) and (27), and then applying Darcy's Law for a similar gradient in potential (i.e., $\nabla\Psi \approx \nabla\Psi_{crack} \approx \nabla\Psi_{aggr}$), we find the transient saturated hydraulic conductivity K_s of the bulk soil to be:

$$K_{fs} = K_{crack,max}\left(\frac{\phi_{crack}(U)}{1-\phi_{sub}(U)}\right)\left(\frac{1-U^q}{1+pU^q}\right) + K_{aggr,max}\left(\frac{1-\beta(U)}{1-\phi_{sub}(U)}\right)\left(\frac{p+1}{p+U^{-q}}\right) \tag{A6}$$

where $K_{crack,max}$ is the maximum hydraulic conductivity of the crack domain (when $U = 0$) and $K_{aggr,max}$ is the maximum hydraulic conductivity of the aggregate domain (when $U = 1$). Note that the only difference between Equation (A6) and Equation (33) is the exponent of 2 applied to $[(1-U^q)/(1+pU^q)]$ in Equation (33). For the six soils analyzed in this study for their transient saturated hydraulic conductivity, the use of Equation (A6) in place of Equation (33) caused only minimal changes in the final model fit (for example, the r^2 value for the Cauquenes silt loam (Chile) soil increased from 0.66 to 0.69 when Equation (A6) was used in place of Equation (33), while the r^2 value for the Limsta clay (Sweden) soil decreased from 0.63 to 0.54). We therefore elected to keep Equation (33) to maintain consistency with the results of *Stewart et al.* [2016],

and to provide a realistic representation of soil crack networks. Nonetheless, Equation (A6) may be preferable in some instances, such as soils that form isolated cracks that do not connect to one another.

Glossary of Terms

u – Gravimetric water content [M M^{-1}]

u_{max} – Maximum (saturated) gravimetric water content [M M^{-1}]

u_{aggr} – Gravimetric water content of the aggregate domain [M M^{-1}]

U – Normalized gravimetric water content of the aggregate domain [-]

V_t – Total volume of the control volume [L^3]

$V_{t,aggr}$ – Total volume of the aggregate domain [L^3]

$V_{t,crack}$ – Total volume of the crack domain [L^3]

$V_{t,sub}$ – Total volume of the subsidence domain [L^3]

V_v – Total volume of voids per unit volume [L^3]

$V_{v,aggr}$ – Volume of aggregate voids per unit volume [L^3]

$V_{v,crack}$ – Volume of crack voids per unit volume [L^3]

$V_{v,sub}$ – Volume of subsidence voids per unit volume [L^3]

$V_{w,aggr}$ – Volume of water within the aggregate domain [L^3]

$V_{w,crack}$ – Volume of water within the crack domain [L^3]

$V_{w,sub}$ – Volume of water within the subsidence domain [L^3]

624 ϕ_{max} – Maximum point of the soil shrinkage curve (assumed to be equal to the total soil porosity)
625 [L^3 L^{-3}]

626 ϕ_{min} – Minimum point of the soil shrinkage curve [L^3 L^{-3}]

627 $\phi_{aggr}(U)$ – Aggregate porosity within the unified porosity framework [L^3 L^{-3}]

628 $\phi_{crack}(U)$ – Shrinkage crack porosity within the unified porosity framework [L^3 L^{-3}]

629 $\phi_{sub}(U)$ – Subsidence porosity within the unified porosity framework [L^3 L^{-3}]

630 $\varepsilon_{aggr}(U)$ – Aggregate porosity within the dual-domain porosity framework [L^3 L^{-3}]

631 $\varepsilon_{crack}(U)$ – Shrinkage crack porosity within the dual-domain porosity framework (assumed to be
632 1) [L^3 L^{-3}]

633 $\beta(U)$ – Weighting factor for the dual porosity domains [L^3 L^{-3}]

634 θ – Volumetric water content within the unified porosity framework [L^3 L^{-3}]

635 θ_{aggr} – Volumetric water content of the aggregates within the unified porosity framework [L^3 L^{-3}]

636 θ_{crack} – Volumetric water content of the cracks within the unified porosity framework [L^3 L^{-3}]

637 θ_{sub} – Volumetric water content of the subsidence domain within the unified porosity framework
638 (assumed to be 0) [L^3 L^{-3}]

639 θ_r – Residual volumetric water content [L^3 L^{-3}]

640 θ_s – Saturated volumetric water content [L^3 L^{-3}]

641 ζ_{aggr} – Volumetric water content of the aggregates within the dual-domain porosity framework
642 [L^3 L^{-3}]

643 ζ_{crack} – Volumetric water content of the cracks within the dual-domain porosity framework [L^3 L^{-3}]

644

645 $\rho_{b,aggr}$ – Bulk density of the soil aggregates [M L^{-3}]

646 ρ_f – Density of the fluid [M L^{-3}]

647 ρ_s – Density of solid particles [M L^{-3}]

648 γ_s – Specific gravity of the solid particles (ρ_s/ρ_f) [M L^3 M^{-1} L^{-3}]

649 g – Gravitational acceleration constant [L T^{-2}]

650 μ_f – Dynamic viscosity of the fluid [M L^{-1} T^{-1}]

651 χ – Shrinkage geometry factor [-]

652 p – Fitting parameter for the soil shrinkage curve [-]

653 q – Fitting parameter for the soil shrinkage curve [-]

654 H_m – Height of an idealized soil matrix, containing aggregates and cracks. Note that H_m varies

655 with the degree of vertical subsidence. [L]

656 M – Number of pores within the aggregate domain [-]

657 N – Number of cracks within the crack domain [-]

658 r_i – Radius of aggregate pore i [L]

659 $r_{i,max}$ – Maximum radius of aggregate pore i [L]

660 $r_{i,min}$ – Minimum radius of aggregate pore i [L]

661 L_j – Length of shrinkage crack j (assumed to be constant) [L]

662 w_j – Width of shrinkage crack j [L]

$w_{j,\max}$ – Maximum width of shrinkage crack j (when $U = 0$) [L]

y_j – Length of shrinkage crack j [L]

$y_{j,\max}$ – Maximum length of shrinkage crack j (when $U = 0$) [L]

τ_i – Tortuosity of aggregate pore i (assumed to be constant) [L L^{-1}]

τ_j – Tortuosity of shrinkage crack j (assumed to be constant) [L L^{-1}]

A_{aggr} – Total cross-sectional area of the aggregate domain [L^2]

A_{crack} – Total cross-sectional area of the crack domain [L^2]

Q – Volumetric water flux through the soil (combined aggregate and crack domains) [L^3 T^{-1}]

Q_{aggr} – Volumetric water flux through the aggregate domain [L^3 T^{-1}]

Q_{crack} – Volumetric water flux through the crack domain [L^3 T^{-1}]

J – Darcian water flux through the soil (combined aggregate and crack domains) [L T^{-1}]

J_{aggr} – Darcian water flux through the aggregate domain [L T^{-1}]

J_{crack} – Darcian water flux through the crack domain [L T^{-1}]

K_s – Transient saturated hydraulic conductivity of the soil (combined aggregate and crack domains); assumed to change with the initial water content of the soil [L T^{-1}]

K_{aggr} – Transient hydraulic conductivity of the aggregate domain [L T^{-1}]

K_{crack} – Transient hydraulic conductivity of the crack domain [L T^{-1}]

$K_{aggr,min}$ – Minimum transient hydraulic conductivity of the aggregate domain (when $U = 0$) [L T^{-1}]

$K_{aggr,max}$ – Maximum transient hydraulic conductivity of the aggregate domain (when $U = 1$) [L T^{-1}]

$K_{crack,max}$ – Maximum transient hydraulic conductivity of the crack domain (when $U = 0$) [L T^{-1}]

$\nabla\Psi$ – Total gradient in potential driving water flow [M L^{-1} T^{-2}]

686 $\nabla\Psi_{aggr}$ – Total gradient in potential driving water flow in the aggregate domain [M L^{-1} T^{-2}]

687 $\nabla\Psi_{crack}$ – Total gradient in potential driving water flow in the crack domain [M L^{-1} T^{-2}]

688 ψ – Soil matric potential [M L^{-1} T^{-2}]

689 α – Parameter for the van Genuchten [1980] water retention curve [L T^2 M^{-1}]

690 m – Parameter for the van Genuchten [1980] water retention curve [-]

691 n – Parameter for the van Genuchten [1980] water retention curve [-]

692 I – Cumulative infiltration [L]

693 S – Soil sorptivity [L $T^{-0.5}$]

694 C – Constant in the family of infiltration solutions based on the two-term Philip model [L]

695 t – Elapsed time in an infiltration experiment [T]

696 a – Constant from the *Wu et al.* [1999] infiltration model (assumed to equal 0.91) [-]

697 f – Parameter from the *Wu et al.* [1999] infiltration model used to account for three-dimensional

698 infiltration effects [L L^{-1}]

699 Λ – Matrix flux potential of the unsaturated soil [L^2 T^{-1}]

700 d – Depth of insertion of the infiltration source (i.e., ring) [L]

701 r_d – Radius of the infiltration source (i.e., ring) [L]

702

703 **Acknowledgments**

704 Data from this paper is permanently archived at https://data.lib.vt.edu/files/s7526c41m and will

705 be provided on request to the corresponding author. Funding for this work was provided in part

706 by the Virginia Agricultural Experiment Station and the Hatch Program of the National Institute

707 of Food and Agriculture, U.S. Department of Agriculture. This material is based upon work

supported by the National Science Foundation under Grant No 0943682. Any opinions, findings, and conclusions or recommendations expressed in this material are those of the authors and do not necessarily reflect the views of the National Science Foundation.

References

Ahuja, L., K. Rojas, J. Hanson, M. Shaffer, and L. Ma (2000), *Root zone water quality model: modelling management effects on water quality and crop production*, Water Resources Publication, Highlands Ranch, CO.

Bagarello, V., S. Di Prima, M. Iovino, and G. Provenzano (2014), Estimating field-saturated soil hydraulic conductivity by a simplified Beerkan infiltration experiment, *Hydrol. Proc.*, *28*(3), 1095-1103.

Bouma, J. (1980), Field measurement of soil hydraulic properties characterizing water movement through swelling clay soils, *J. Hydrol.*, *45*(1), 149-158.

Braud, I., D. De Condappa, J. M. Soria, R. Haverkamp, R. Angulo-Jaramillo, S. Galle, and M. Vauclin (2005), Use of scaled forms of the infiltration equation for the estimation of unsaturated soil hydraulic properties (the Beerkan method), *European J. Soil Sci.*, *56*(3), 361-374.

Bronswijk, J. (1990), Shrinkage geometry of a heavy clay soil at various stresses, *Soil Sci. Soc. Amer. J.*, *54*(5), 1500-1502.

Castiglione, P., B. P. Mohanty, P. J. Shouse, J. Simunek, M. T. van Genuchten, and A. Santini (2003), Lateral Water Diffusion in an Artificial Macroporous System: Modeling and Experimental Evidence, *Vadose Zone J.*, *2*(2), 212-221.

730 Chen, C., and R. Wagenet (1992), Simulation of water and chemicals in macropore soils Part 1.
731 Representation of the equivalent macropore influence and its effect on soilwater flow,
732 *J.Hydrol.*, *130*(1), 105-126.
733 Coppola, A., H. H. Gerke, A. Comegna, A. Basile, and V. Comegna (2012), Dual-permeability
734 model for flow in shrinking soil with dominant horizontal deformation, *Water Resourc.*
735 *Res.*, *48*(8), W08527.
736 Coppola, A., A. Comegna, G. Dragonetti, H. H. Gerke, and A. Basile (2015), Simulated
737 Preferential Water Flow and Solute Transport in Shrinking Soils, *Vadose Zone J*. 14(9),
738 1-22.
739 Corbeels, M., R. Hartmann, G. Hofman, and O. Van Cleemput (1999), Field calibration of a
740 neutron moisture meter in vertisols, *Soil Sci. Soc. Amer. J.*, *63*(1), 11-18.
741 Das Gupta, S., B. P. Mohanty, and J. M. Köhne (2006), Soil hydraulic conductivities and their
742 spatial and temporal variations in a vertisol, *Soil Sci. Soc. Amer. J.*, *70*(6), 1872-1881.
743 Davidson, M. R. (1984), A Green-Ampt Model of infiltration in a cracked soil, *Water Resourc.*
744 *Res.*, *20*(11), 1685-1690.
745 Dunn, G. H., and R. E. Phillips (1991), Equivalent Diameter of Simulated Macropore Systems
746 during Saturated Flow, *Soil Sci. Soc. Amer. J.*, *55*(5), 1244-1248.
747 Gerke, H. H. (2006), Preferential flow descriptions for structured soils, *J. Plant Nutrit. Soil Sci.*,
748 *169*(3), 382-400.
749 Gerke, H. H., and M. T. van Genuchten (1993), A dual-porosity model for simulating the
750 preferential movement of water and solutes in structured porous media, *Water Resourc.*
751 *Res.*, *29*(2), 305-319.

752 Gerke, H. H., and J. M. Köhne (2004), Dual-permeability modeling of preferential bromide
753 leaching from a tile-drained glacial till agricultural field, *J. Hydrol.*, *289*(1-4), 239-257.
754 Greco, R. (2002), Preferential flow in macroporous swelling soil with internal catchment: model
755 development and applications, *J. Hydrol.*, *269*(3), 150-168.
756 Gwo, J., P. Jardine, G. Wilson, and G. Yeh (1995), A multiple-pore-region concept to modeling
757 mass transfer in subsurface media, *J. Hydrol.*, *164*(1), 217-237.
758 Haverkamp, R., F. Bouraoui, C. Zammit, and R. Angulo-Jaramillo (1998), Soil properties and
759 moisture movement in the unsaturated zone, in *Handbook of Groundwater Engineering*,
760 edited by J. Delleur, CRC Press, Boca Raton, Florida, 5:1-50.
761 Horn, R., X. Peng, H. Fleige, and J. Dörner (2014), Pore rigidity in structured soils—only a
762 theoretical boundary condition for hydraulic properties?, *Soil Sci. Plant Nutr.*, *60*(1), 3-
763 14.
764 Hutson, J., and R. Wagenet (1995), A multiregion model describing water flow and solute
765 transport in heterogeneous soils, *Soil Sci. Soc. Amer. J.*, *59*(3), 743-751.
766 Jabro, J. D. (1996), Variability of field-saturated hydraulic conductivity in a Hagerstown soil as
767 affected by initial water content, *Soil Sci.*, *161*(11), 735-739.
768 Jarvis, N. J. (2007), A review of non-equilibrium water flow and solute transport in soil
769 macropores: principles, controlling factors and consequences for water quality, *European*
770 *J. Soil Sci.*, *58*(3), 523-546.
771 Klute, A., and C. Dirksen (1986), Hydraulic conductivity and diffusivity: Laboratory methods,
772 *Methods of Soil Analysis: Part 1—Physical and Mineralogical*
773 *Methods*(methodsofsoilan1), 687-734.

774 Knezevich, C. A. (1975), *Soil Survey of Benton County Area, Oregon*, US Soil Conservation
775 Service, Washington, DC.
776 Kutílek, M. (1996), Water relations and water management of vertisols, *Developments in Soil*
777 *Science*, *24*, 201-230.
778 Larsbo, M., and N. Jarvis (2003), *MACRO 5.0: a model of water flow and solute transport in*
779 *macroporous soil: technical description*, Department of Soil Sciences, Swedish
780 University of Agricultural Sciences, Uppsala, Sweden.
781 Larsbo, M., S. Roulier, F. Stenemo, R. Kasteel, and N. Jarvis (2005), An Improved Dual-
782 Permeability Model of Water Flow and Solute Transport in the Vadose Zone, *Vadose*
783 *Zone J.*, *4*(2), 398.
784 Lassabatère, L., D. Yilmax, X. Peyrard, P. Peyneau, T. Lenoir, J. Simunek, and R. Angulo
785 Jaramillo (2014), New Analytical Model for Cumulative Infiltration into Dual-
786 Permeability Soils, *Vadose Zone J.*, *13*(12), 1-15.
787 Lin, H., K. Mclnnes, L. Wilding, and C. Hallmark (1998), Macroporosity and initial moisture
788 effects on infiltration rates in vertisols and vertic intergrades, *Soil Sci.*, *163*(1), 2-8.
789 Messing, I., and N. J. Jarvis (1990), Seasonal variation in field-saturated hydraulic conductivity
790 in two swelling clay soils in Sweden, *J. Soil Sci.*, *41*(2), 229-237.
791 Morel-Seytoux, H. J., P. D. Meyer, M. Nachabe, J. Touma, M. T. van Genuchten, and R. J.
792 Lenhard (1996), Parameter equivalence for the Brooks-Corey and van Genuchten soil
793 characteristics: Preserving the effective capillary drive, *Water Resourc. Res.*, *32*(5), 1251-
794 1258.
795 Nimmo, J. R. (2010), Theory for source-responsive and free-surface film modeling of
796 unsaturated flow, *Vadose Zone J.*, *9*(2), 295-306.

797 Nimmo, J. R. (2016), Quantitative Framework for Preferential Flow Initiation and Partitioning,
798 *Vadose Zone J.*, *15*(2), 1-12.
799 Novák, V., J. Šimůnek, and M. T. Van Genuchten (2002), Infiltration into a swelling, cracked
800 clay soil, *J. Hydrol. Hydromech.*, *50*(1), 3-19.
801 Peters, R. R., and E. A. Klavetter (1988), A continuum model for water movement in an
802 unsaturated fractured rock mass, *Water Resourc. Res.*, *24*(3), 416-430.
803 Reynolds, W. D., B. T. Bowman, R. R. Brunke, C. F. Drury, and C. S. Tan (2000), Comparison
804 of Tension Infiltrometer, Pressure Infiltrometer, and Soil Core Estimates of Saturated
805 Hydraulic Conductivity, *Soil Sci. Soc. Amer. J.*, *64*(2), 478-484.
806 Römkens, M. J. M., and S. N. Prasad (2006), Rain Infiltration into swelling/shrinking/cracking
807 soils, *Agricult. Water Manage.*, *86*(1-2), 196-205.
808 Simunek, J., N. J. Jarvis, M. T. van Genuchten, and A. Gärdenäs (2003), Review and comparison
809 of models for describing non-equilibrium and preferential flow and transport in the
810 vadose zone, *J. Hydrol.*, *272*, 14-35.
811 Smiles, D. E., and J. H. Knight (1976), A note on the use of the Philip infiltration equation, *Soil*
812 *Res.*, *14*(1), 103-108.
813 Stewart, R. D., M. R. Abou Najm, D. E. Rupp, and J. S. Selker (2012), An Image-Based Method
814 for Determining Bulk Density and the Soil Shrinkage Curve, *Soil Science Society of*
815 *America Journal*, *76*(4), 1217-1221.
816 Stewart, R. D., M. R. Abou Najm, D. E. Rupp, J. W. Lane, H. C. Uribe, J. L. Arumí, and J. S.
817 Selker (2015), Hillslope runoff thresholds with shrink-swell clay soils, *Hydrol.*
818 *Processes*, *29*(4), 557-571.

819 Stewart, R. D., D. E. Rupp, M. R. Abou Najm, and J. S. Selker (2016), A Unified Model for Soil
820 Shrinkage, Subsidence, and Cracking, *Vadose Zone J.*, *15*(3), 1-15.
821 Sukop, M. C., H. Huang, P. F. Alvarez, E. A. Variano, and K. J. Cunningham (2013), Evaluation
822 of permeability and non‐Darcy flow in vuggy macroporous limestone aquifer samples
823 with lattice Boltzmann methods, *Water Resourc. Res.*, *49*(1), 216-230.
824 Tsang, Y. W., and C. F. Tsang (1987), Channel model of flow through fractured media, *Water*
825 *Resourc. Res.*, *23*(3), 467-479.
826 van Genuchten, M. T. (1980), A closed-form equation for predicting the hydraulic conductivity
827 of unsaturated soils, *Soil Science Society of America Journal*, *44*(5), 892-898.
828 Wu, L., L. Pan, J. Mitchell, and B. Sanden (1999), Measuring saturated hydraulic conductivity
829 using a generalized solution for single-ring infiltrometers, *Soil Sci. Soc. Amer. J.*, *63*(4),
830 788-792.
831
832

Tables

Table 1 – Summary of model parameters for the seven soils included in this study. u_{max} is the maximum gravimetric water content; ϕ_{max} is the total porosity of the control volume; ϕ_{min} is the minimum porosity of the aggregate domain; p and q are fitting parameters for the soil shrinkage curve; $K_{crack,max}$ is the maximum hydraulic conductivity of the shrinkage crack domain; and $K_{aggr,max}$ is the maximum hydraulic conductivity of the aggregate domain. r^2 refers to the coefficient of determination between the observed K_s values in each study versus the K_s values predicted by Equation (33). The range of parameters associated with a 95% confidence interval is indicated in parentheses; NA values signify instances where the lower parameter bound was not able to be determined. Note that the shrinkage geometry factor χ was assumed to equal 3 for all samples (isotropic shrinkage).

Soil	**Source**	u_{max} g g^{-1}	ϕ_{max} m m^{-3}	ϕ_{min} m m^{-3}	p -	q -	$K_{aggr,max}$ mm hr^{-1}	$K_{crack,max}$ mm hr^{-1}	r^2 -
1. Haplic Spagnosol (Germany)	*Horn et al.*, 2014	0.43	0.54	0.20	1.9 (0.73; 3.8)	3.2 (2.4; 4.1)	-	-	-
2. Chromic Calcixerert (Morocco)	*Corbeels et al.*, 1999	0.39	0.56	0.26	0.31 (NA; 1.2)	2.7 (2.1; 3.6)	-	-	-
3. Waldo silty clay loam (OR)	*Stewart et al.*, 2016	0.57	0.60	0.19	3.0 (1.5; 5.2)	2.2 (1.8; 2.6)	3.4 (NA; 17)	3500 (1200; 7600)	0.74
4. Cauquenes loam (Chile)	*Stewart et al.*, 2016	0.48	0.57	0.23	6.6 (NA; 140)	2.3 (0.94; 4.7)	6.9 (4.3; 11)	220 (160; 310)	0.66
5. Ultana clay (Sweden)	*Messing and Jarvis*, 1990	0.39	0.51	0.27	1.3 (0.30; 3.2)	3.0 (2.2; 3.8)	52 (NA; 390)	630 (110; 2100)	0.10
6. Limsta clay (Sweden)	*Messing and Jarvis*, 1990	0.44	0.54	0.28	2.0 (1.0; 3.6)	4.1 (3.3; 4.9)	0.74 (NA; 9.7)	310 (83; 2000)	0.63
7. Hagerstown silt loam (PA)	*Jabro*, 1996	0.21	0.36	0.22	7.0 (2.0; 22)	12 (6.4; 18)	$3.1\text{x}10^{-5}$ ($1.9; 4.3$) $\text{x}10^{-5}$	0.023 (0.016; 0.039)	0.91
8. Ships clay (TX)	*Lin et al.*, 1998	0.47	0.56	0.22	0.38 (0; 2.3)	2.3 (0; 5.0)	0.010 (0.0050; 0.015)	3.85 (1.9; 5.8)	0.99

842 **Figures**

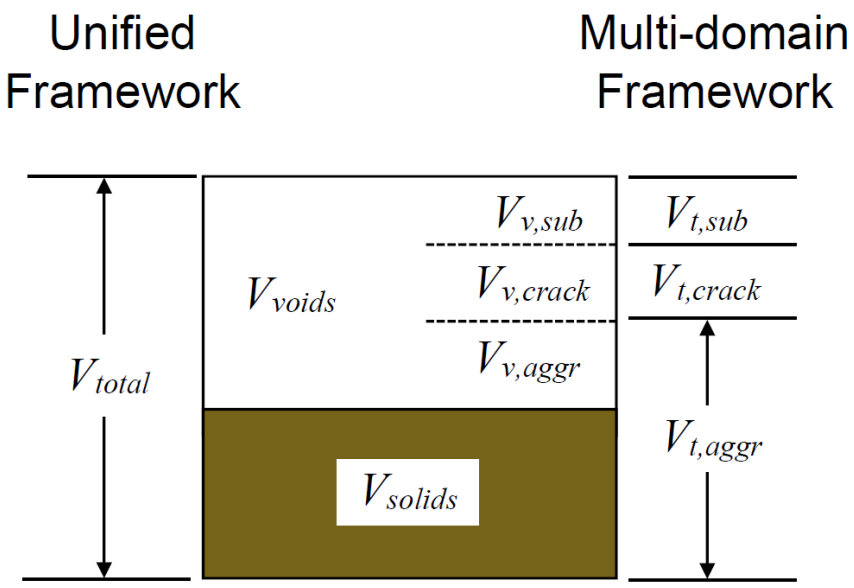

843

844 Figure 1 – Representation of the division of a soil control volume into various domains,
845 including subsidence (*sub*), cracks (*crack*) and aggregates (*aggr*). The unified framework relates
846 all domains to the total control volume (V_{total}) while the dual-domain framework treats each
847 domain independently. Note that *V* refers to volume, while the subscripts *v* and *t* respectively
848 refer to voids and total.

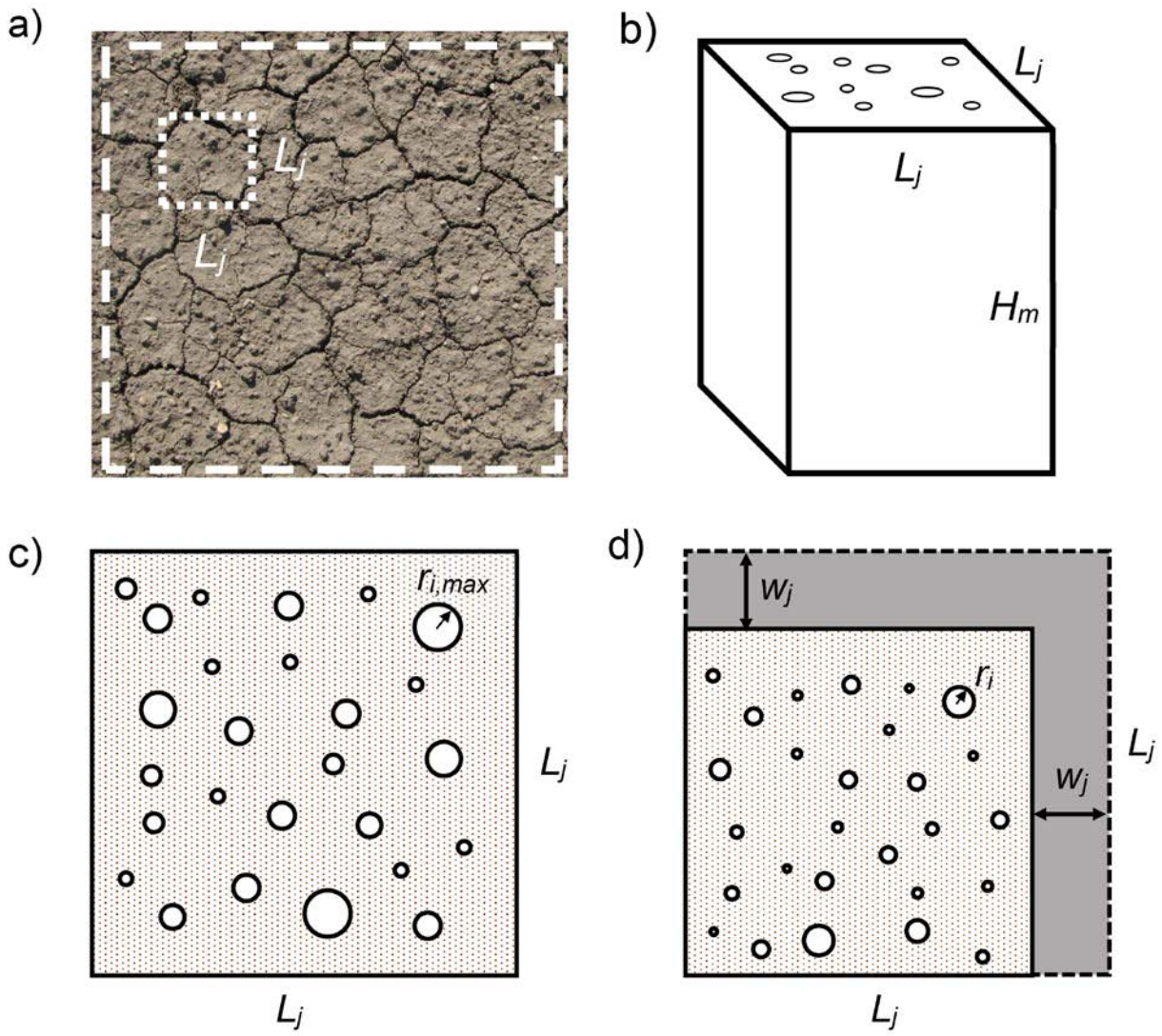

Figure 2 – a) Example of a shrink-swell soil control volume (outer dashed box), with soil block *j* identified by the small dotted white box; b) conceptualization of soil block *j* as a three-dimensional cube of dimensions L_j x L_j x H_m; c) overhead view of soil block *j* in saturated conditions (U = 1), showing aggregate pores as cylindrical tubes (note that example pore r_i is shown at its maximum size, $r_{i,max}$); d) overhead view of soil block *j* in unsaturated conditions (U < 1), showing aggregate pores as cylindrical tubes and soil cracks around the perimeter of soil block *j*. Note that the block height H_m will vary depending on the degree of surface subsidence.

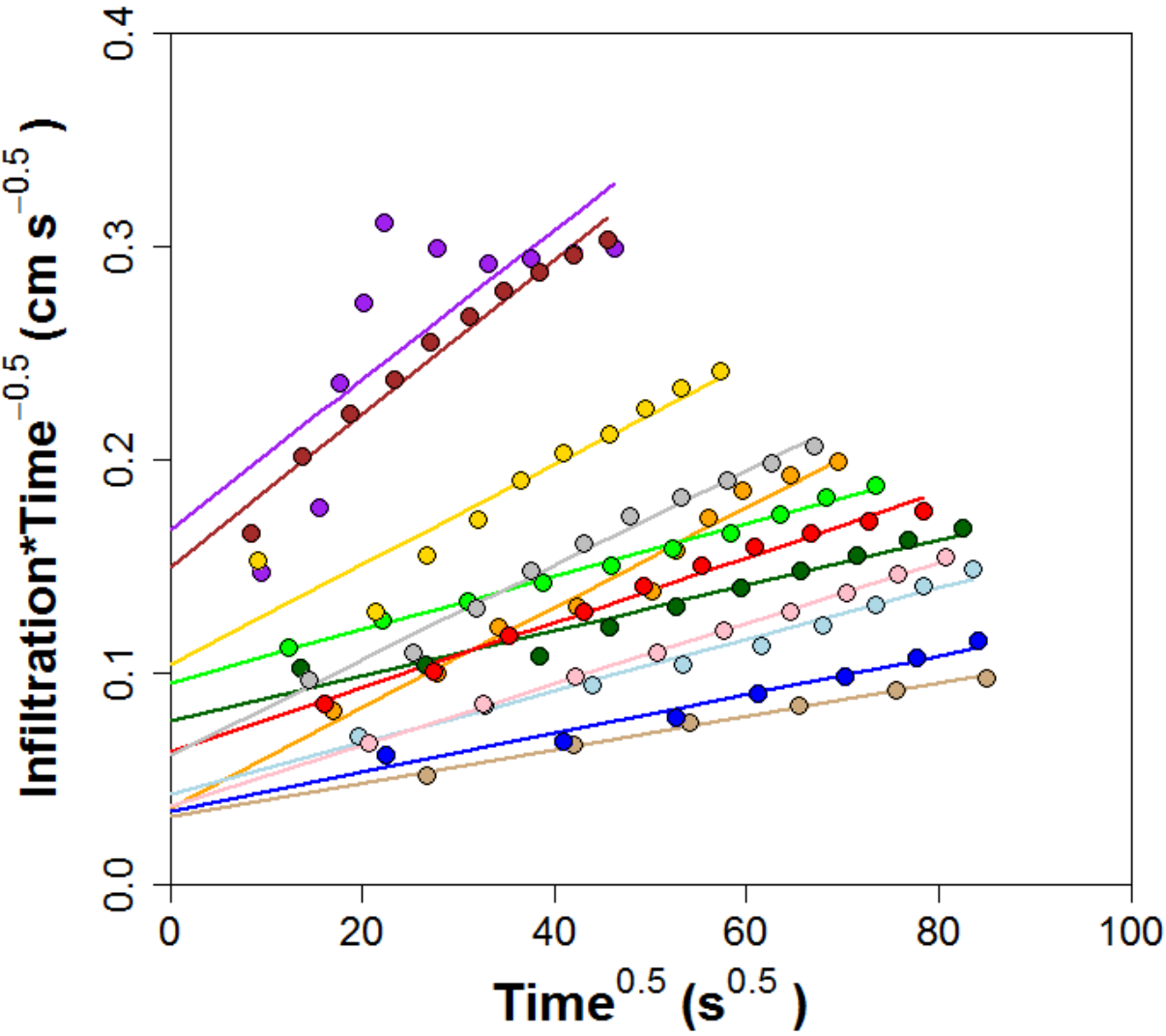

857

858 Figure 3 – Example of infiltration measurements (cumulative infiltration versus time) collected

859 at the Oregon site on May 8, 2012. Twelve infiltration rings (4.6 cm diameter) were used within

860 a 2 x 3 m array. Solid lines represent the model fit using Equation (34).

861

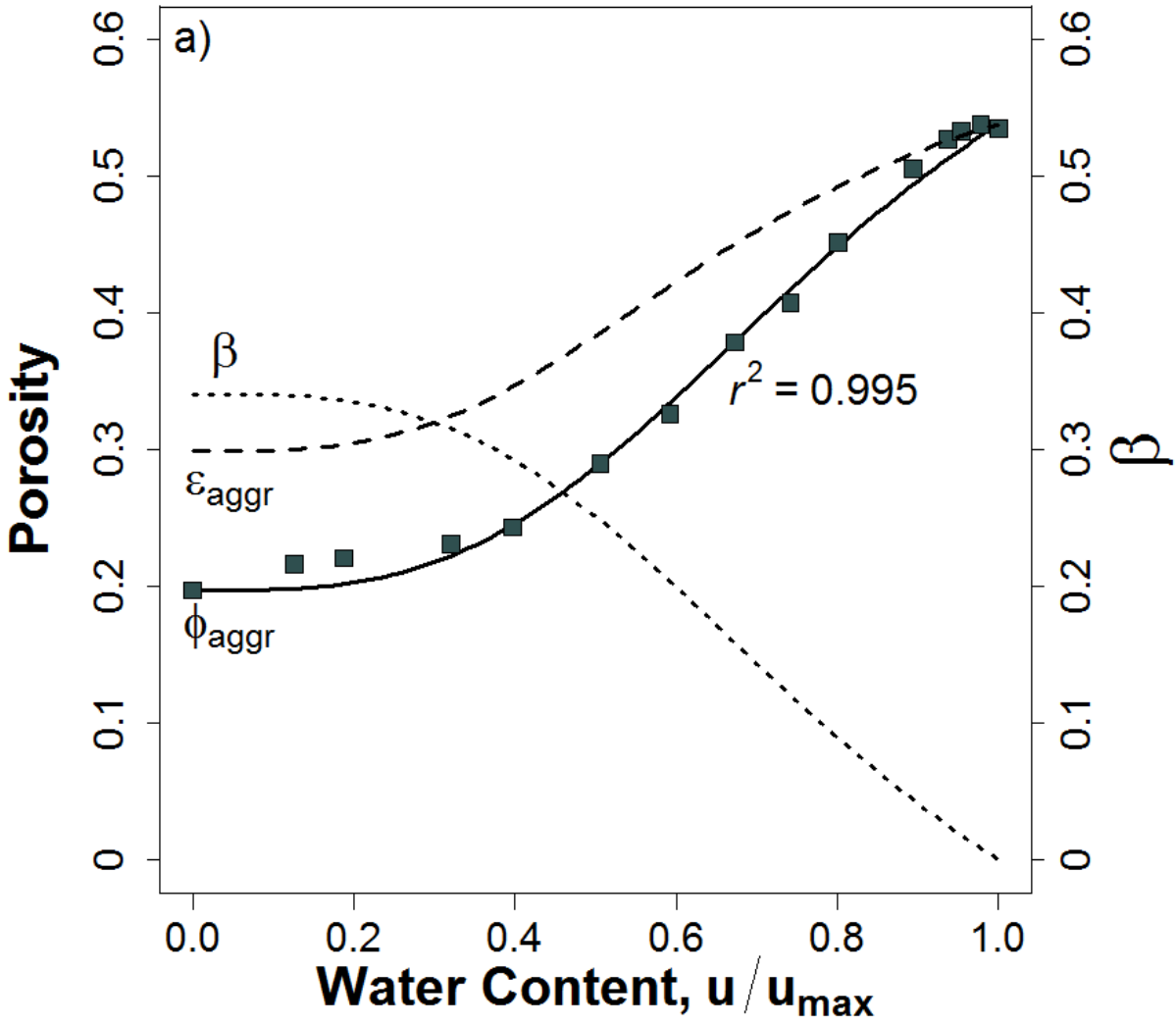
a)
Porosity
β
ε_{aggr}
ϕ_{aggr}
r^2 = 0.995
β
0
0.1
0.2
0.3
0.4
0.5
0.6
0.0
0.2
0.4
0.6
0.8
1.0
Water Content, u / u_{max}

862

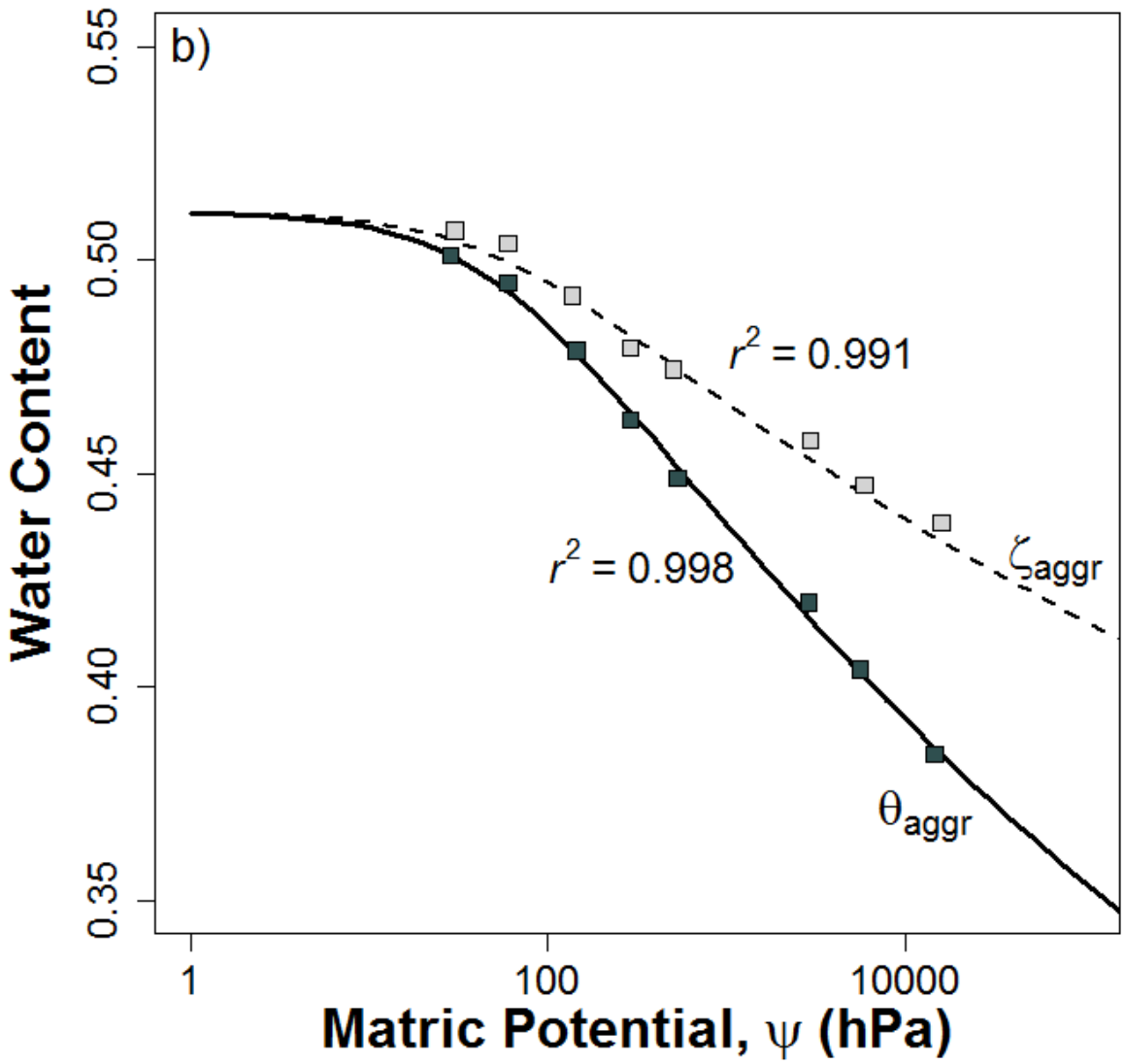

Figure 4 – Measured and modeled a) soil shrinkage, and b) water retention of a Haplic Stagnosol clay soil, originally reported by Horn et al. (2014). The solid line in a) represents Equation (2), the dotted line represents Equation (8) and the dashed line represents Equation (9). The dark gray points in b) represent the measured water content assuming that the sample volume does not change (i.e., θ_{aggr}), while the light gray points represent the measured water content accounting for measured soil shrinkage (i.e., ζ_{aggr}). The dark line represents the van Genuchten (1980) water retention model, while the dashed line represents Equation (12).

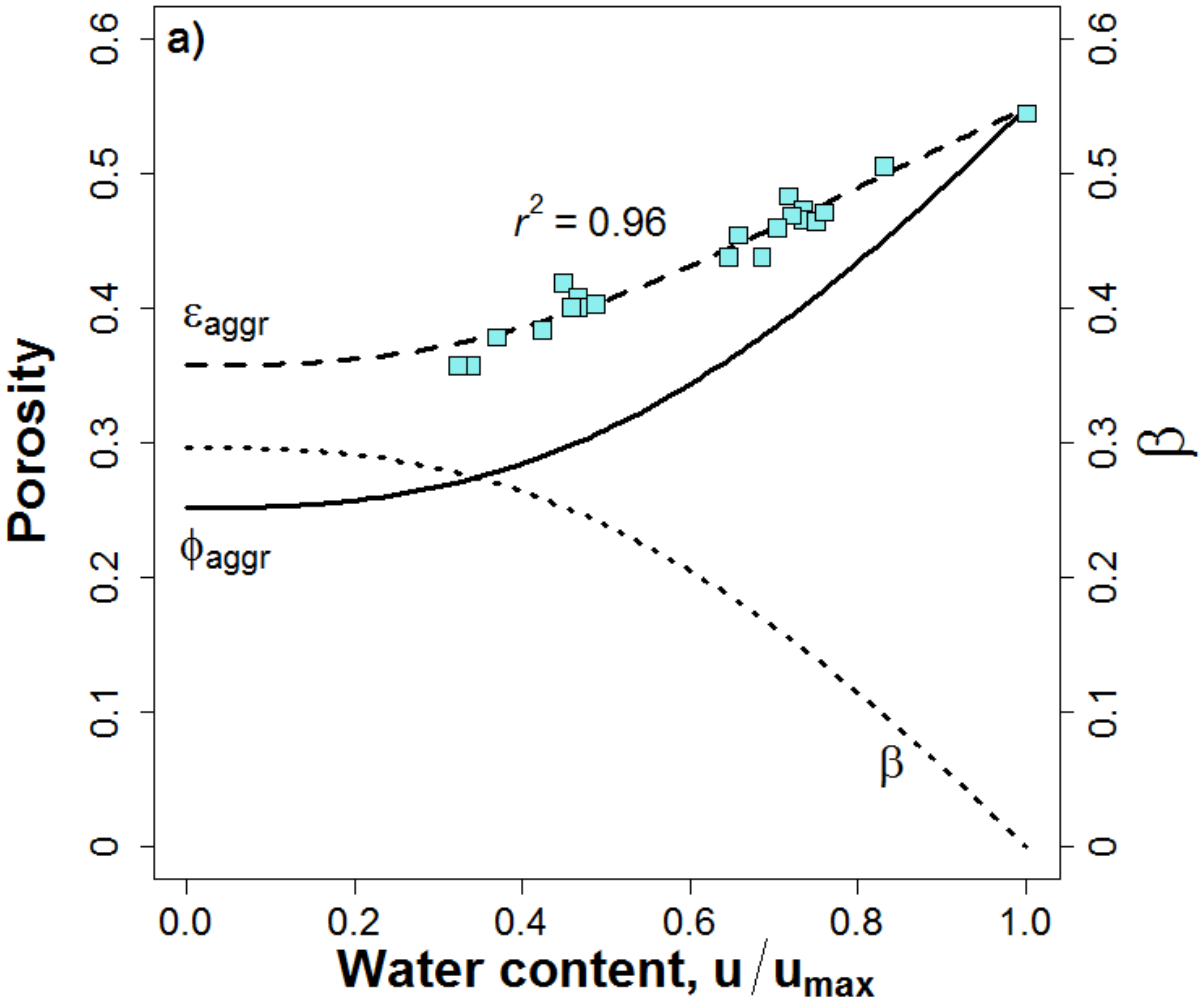
a)
r^2 = 0.96
ε_{aggr}
ϕ_{aggr}
β
Porosity
β
Water content, u / u_{max}
0.0
0.2
0.4
0.6
0.8
1.0
0
0.1
0.2
0.3
0.4
0.5
0.6

871

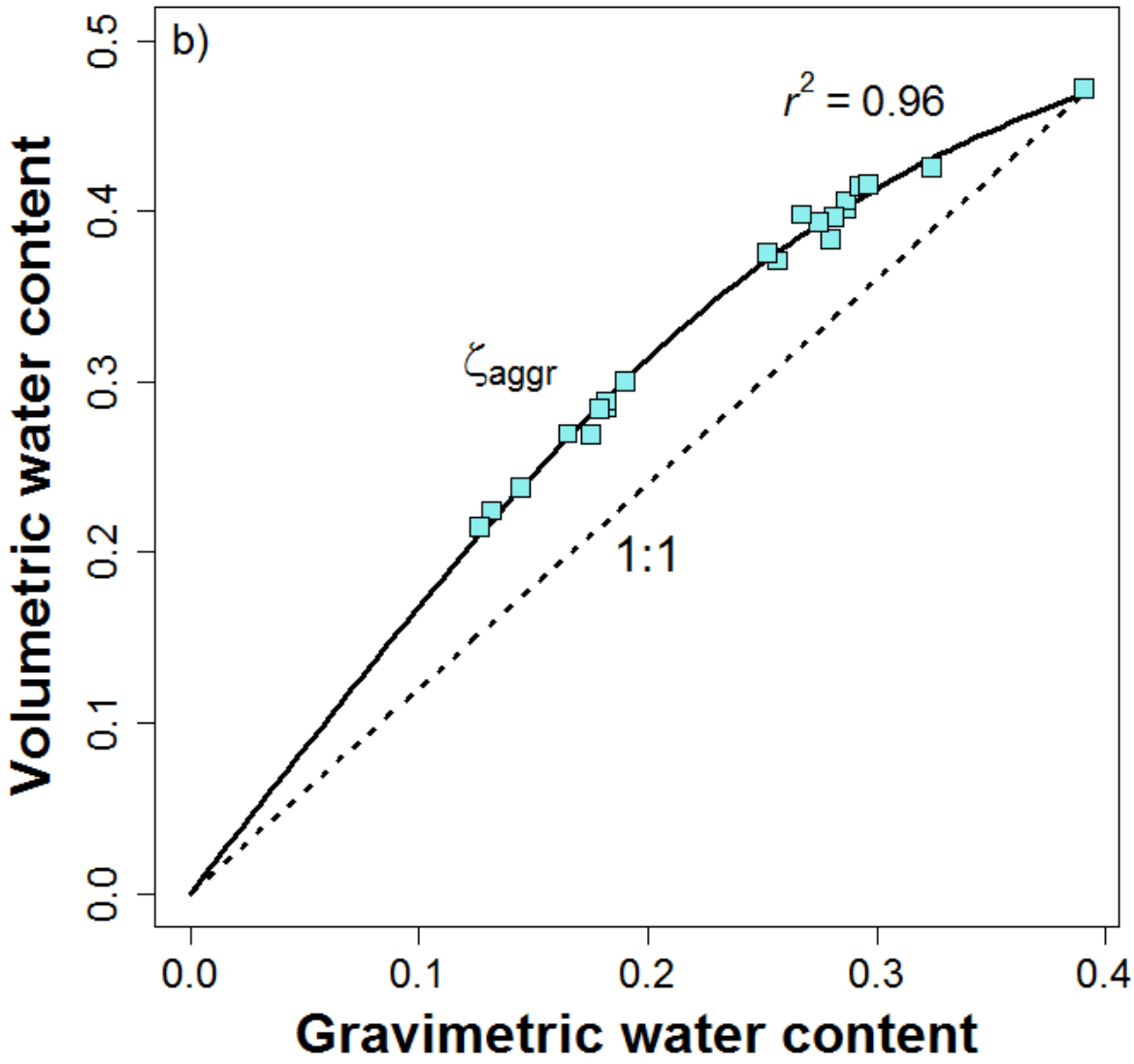

872

873 Figure 5 – a) Soil shrinkage curve for the Chromic Calcixerert (Morocco) soil. Data points are
874 from *Corbeels et al.* [1999], where the authors measured aggregate bulk density as a function of
875 gravimetric water content. Note that the solid line represents Equation (2), the dotted line
876 represents Equation (8) and the dashed line represents Equation (9). b) Relationship between
877 domain-dependent aggregate volumetric water content (ζ_{aggr}) and gravimetric water content (u)
878 of the Chromic Calcixerert (Morocco) soil. The solid line represents Equation (13).

879

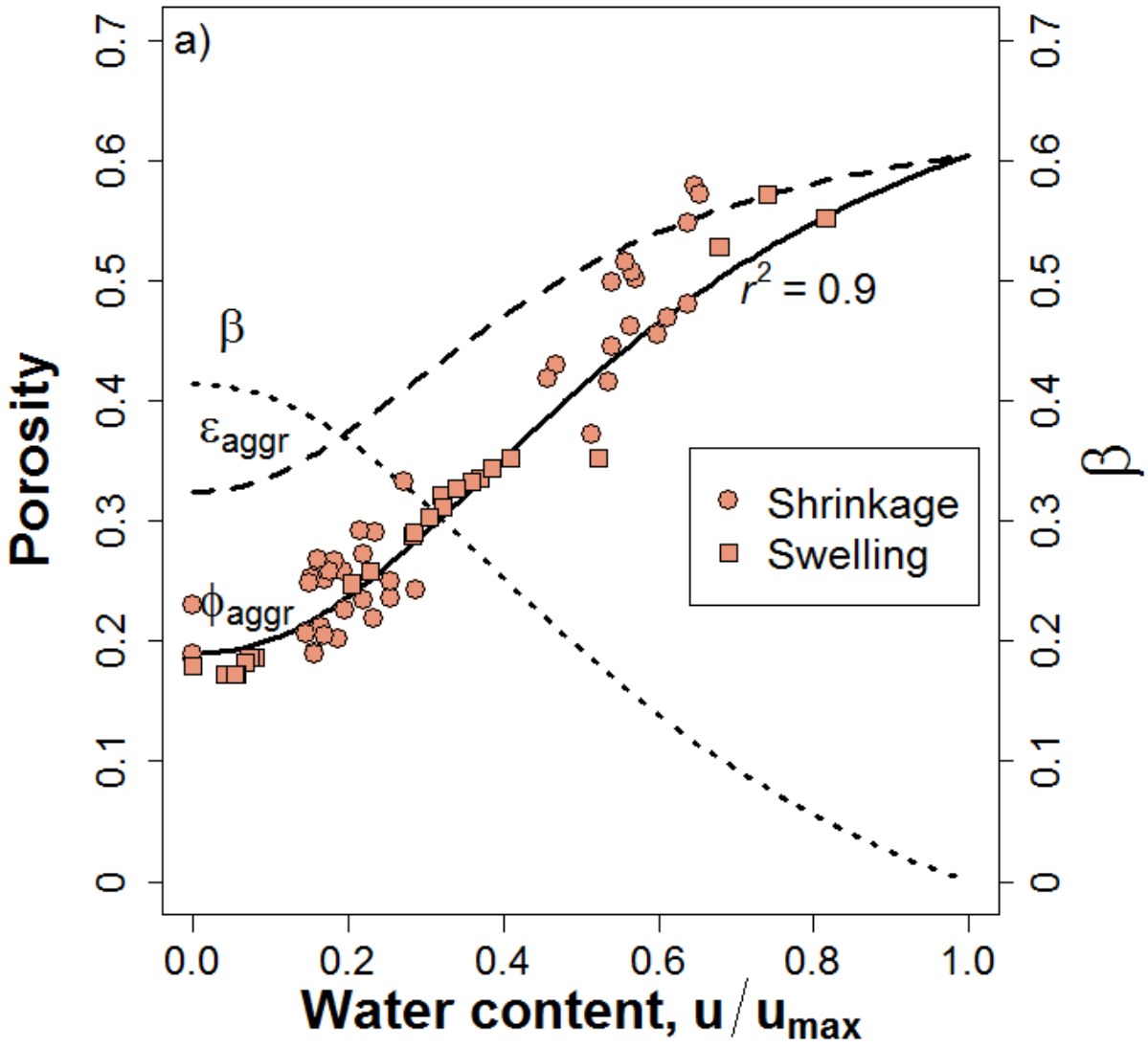
a)
Porosity
β
ε_{aggr}
ϕ_{aggr}
r^2 = 0.9
Shrinkage
Swelling
β
Water content, u / u_{max}
0.0
0.2
0.4
0.6
0.8
1.0
0
0.1
0.2
0.3
0.4
0.5
0.6
0.7

880

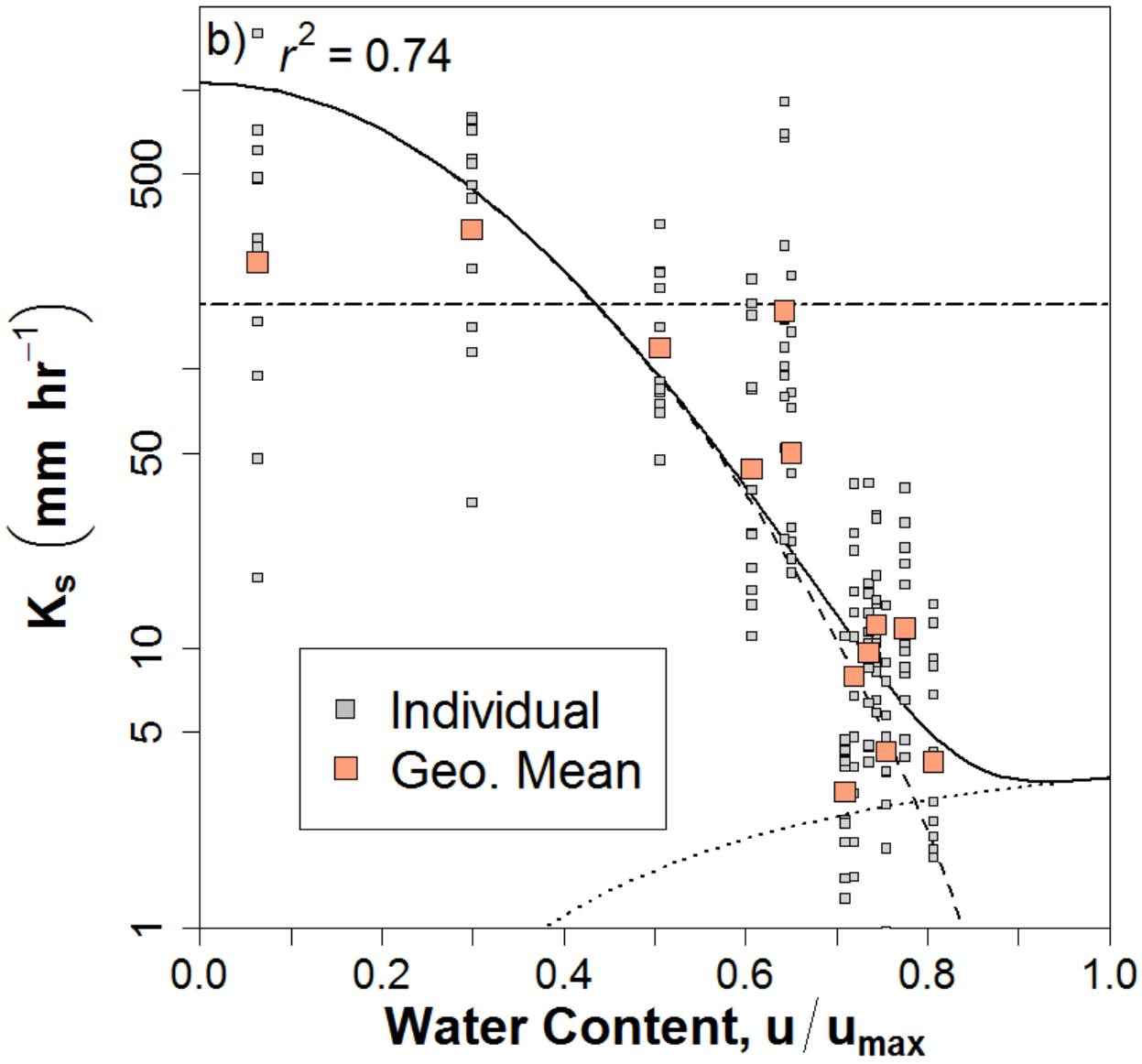

881

882 Figure 6 – a) Soil shrinkage curve for the Waldo silty clay loam (Oregon) soil. The solid line
883 represents Equation (2), the dotted line represents Equation (8) and the dashed line represents
884 Equation (9). b) Transient saturated hydraulic conductivity values estimated from single ring
885 infiltration measurements taken at the Oregon field site. K_s values were estimated using the *Wu*
886 *et al.* [1999] infiltration model. The solid line shows the prediction of Equation (33); the dashed
887 line shows the crack contribution to K_s and the dotted line shows the aggregate contribution to

888 K_s. The dash-dotted line shows the laboratory measurement of K_s using cores and assuming a

889 constant value.

890

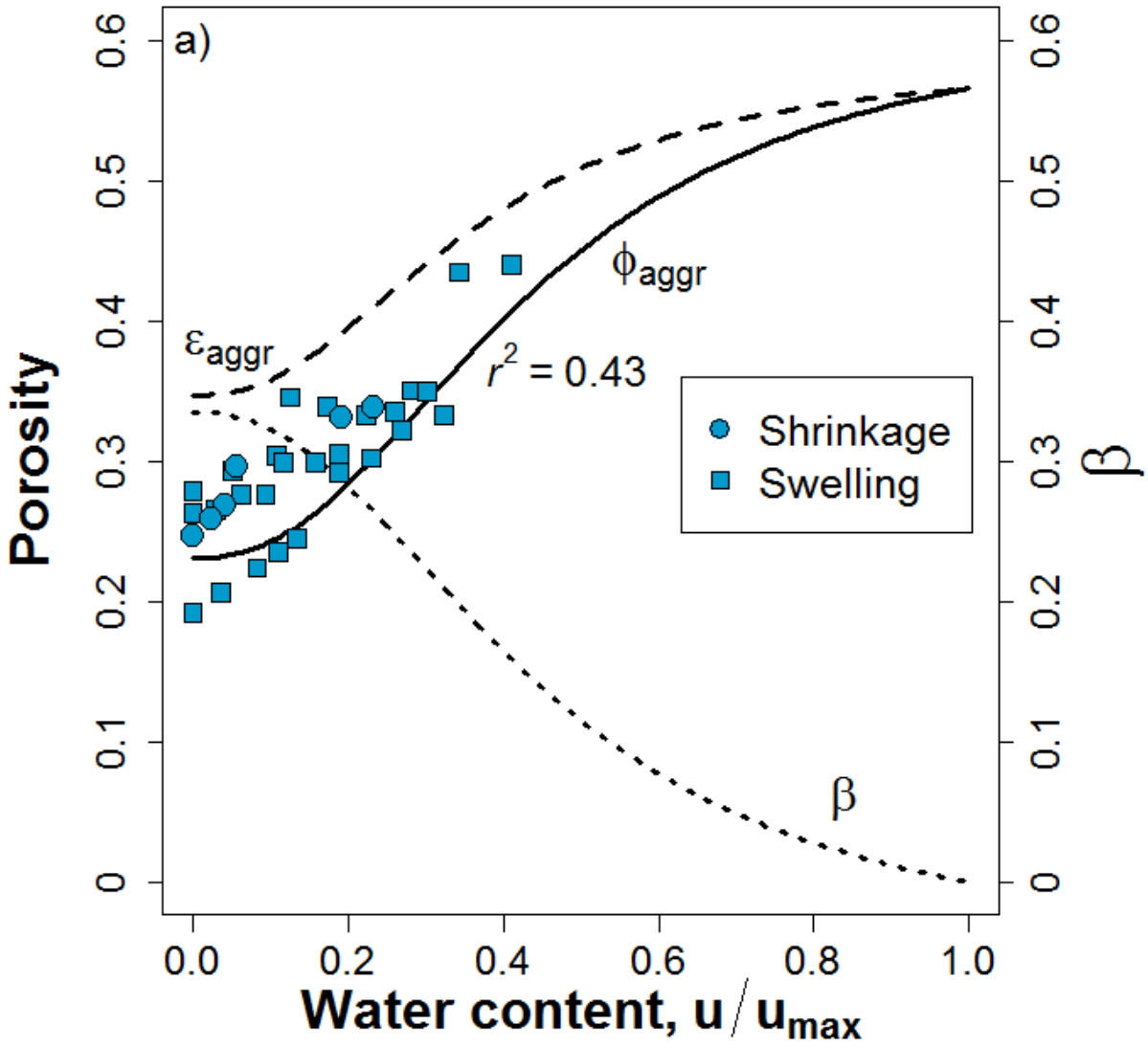
a)
Porosity
Water content, u / u_max
ε_aggr
ϕ_aggr
r² = 0.43
Shrinkage
Swelling
β
β
0
0.1
0.2
0.3
0.4
0.5
0.6
0.0
0.2
0.4
0.6
0.8
1.0

891

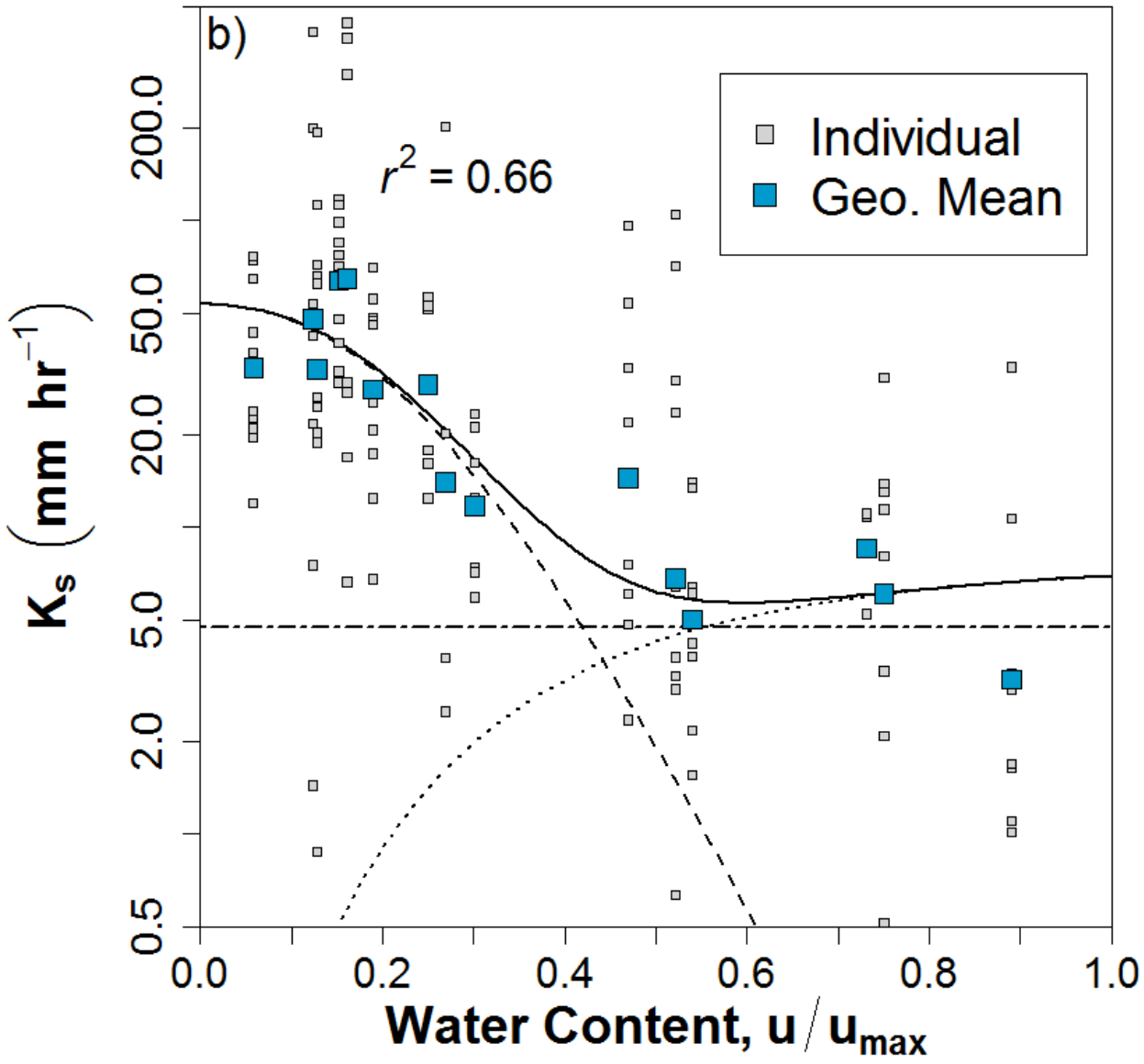

892

893 Figure 7 – a) Soil shrinkage curve for the Cauquenes loam (Chile) soil. The solid line represents
894 Equation (2), the dotted line represents Equation (8) and the dashed line represents Equation (9).
895 b) Transient saturated hydraulic conductivity values estimated from single ring infiltration
896 measurements taken at the Chile field site. K_s values were estimated using the *Wu et al.* [1999]
897 infiltration model. The solid line shows the prediction of Equation (33); the dashed line shows
898 the crack contribution to K_s and the dotted line shows the aggregate contribution to K_s. The dash-

899 dotted line indicates the K_s value measured on laboratory cores, assuming a constant value for all

900 initial water contents.

901

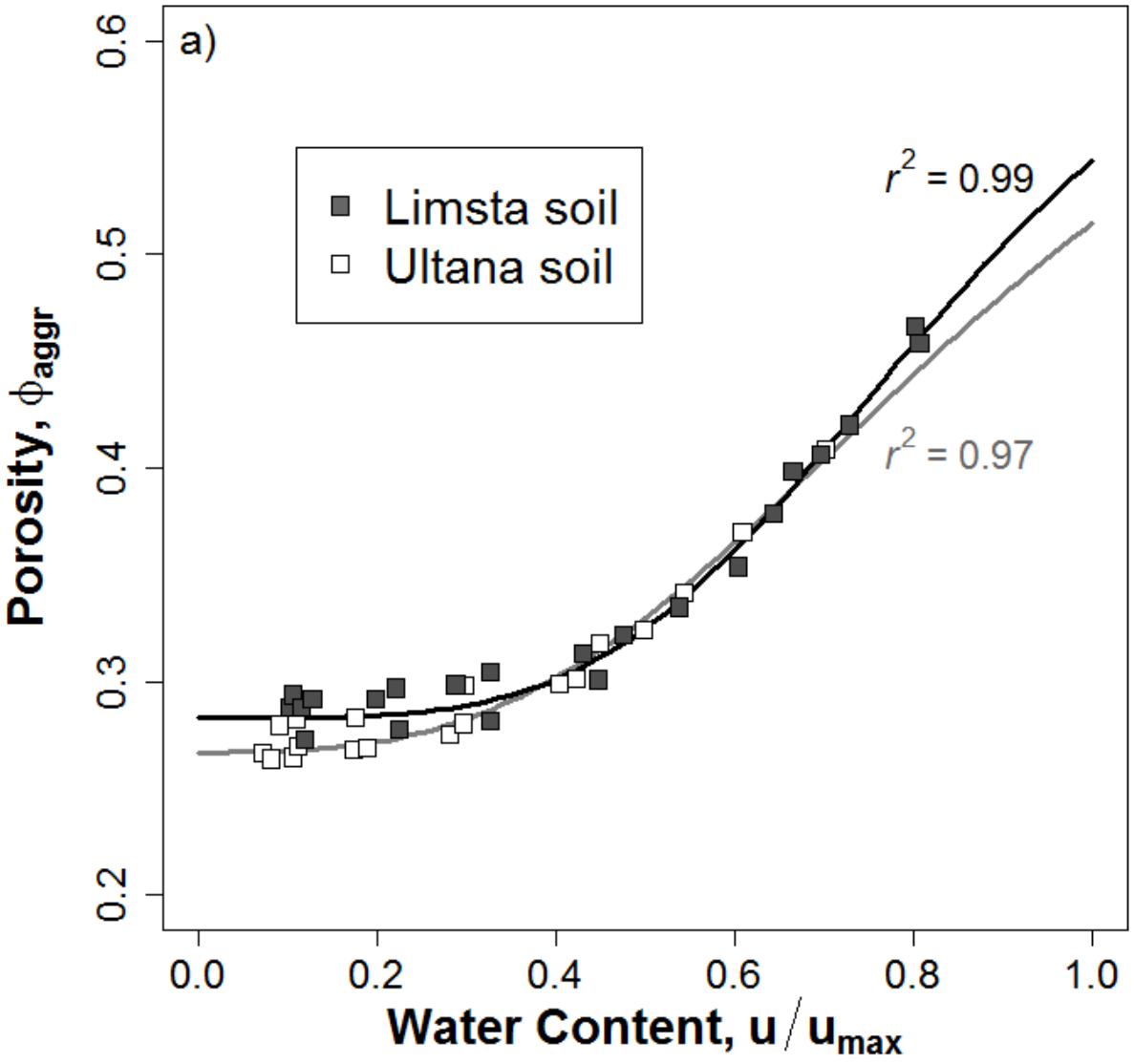
a)
Limsta soil
Ultana soil
r^2 = 0.99
r^2 = 0.97
Porosity, ϕ_{aggr}
0.2
0.3
0.4
0.5
0.6
0.0
0.2
0.4
0.6
0.8
1.0
Water Content, u / u_{max}

902

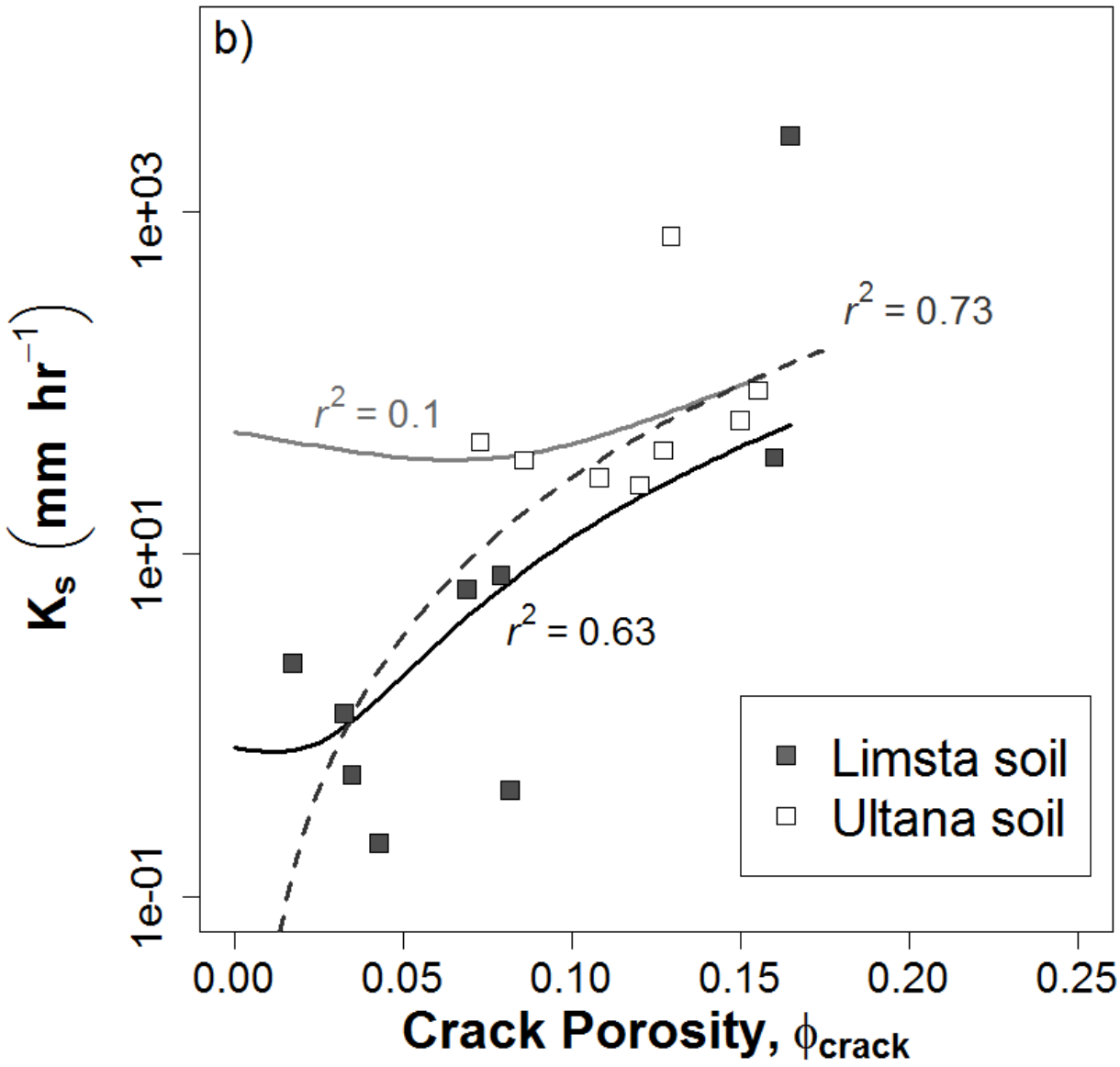

903

904 Figure 8 – a) Soil shrinkage curves showing the relationship between water content, u/u_{max}, and
905 aggregate porosity, ϕ_{aggr}, and b) Transient saturated hydraulic conductivity, K_s, versus crack
906 porosity, ϕ_{crack}, for soils at two Swedish sites (Limsta and Ultana). Data points come from
907 *Messing and Jarvis* [1990]. Solid lines in a) represent predictions of Equation (2) and in b)
908 represent the predictions of Equation (33). The dashed line in b) represents the model fit when
909 the two soils are combined, as was done in the original source.

910

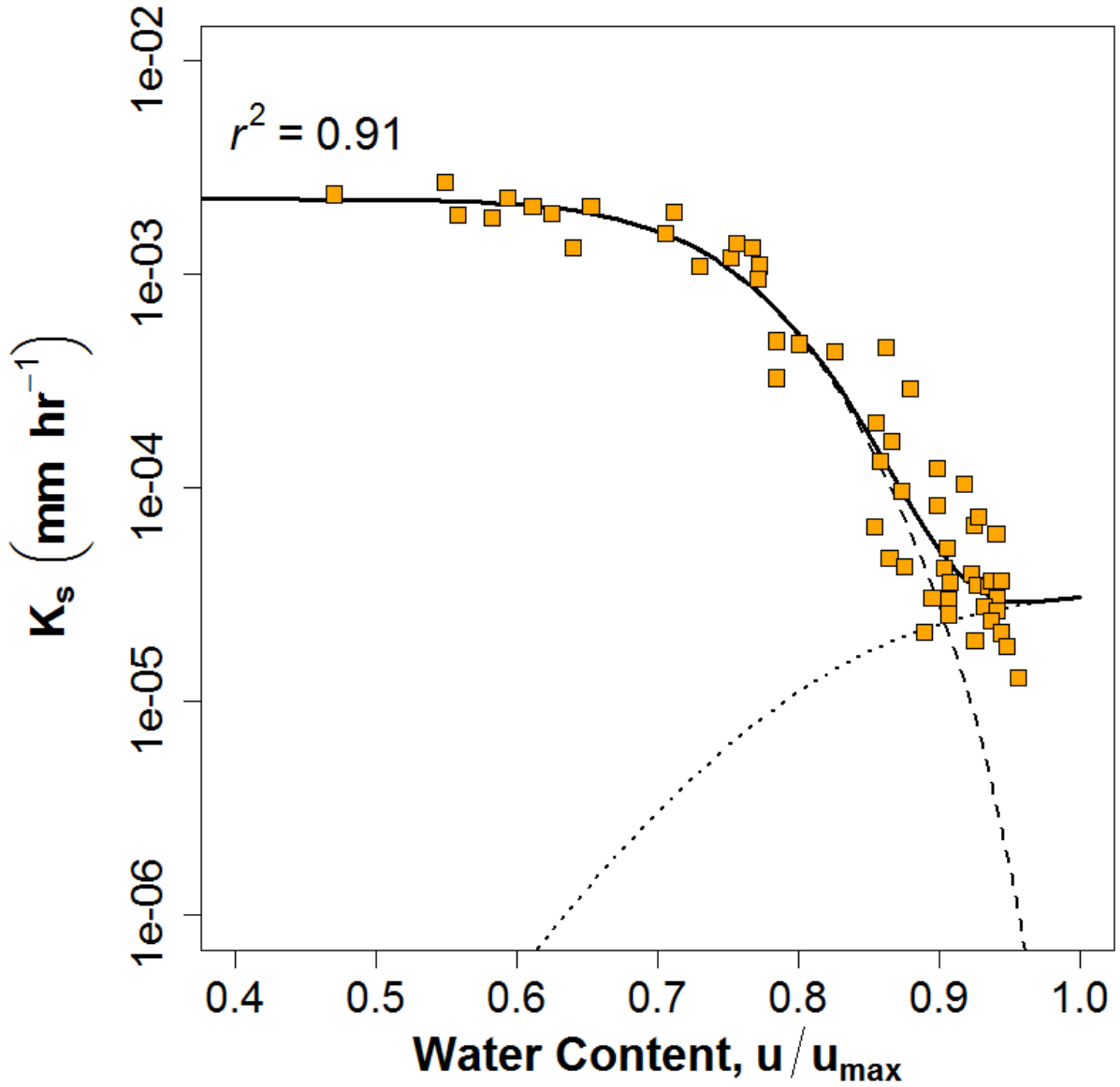

911

912 Figure 9 – Transient saturated hydraulic conductivity (K_s) versus water content (u/u_{max}) for a
913 Hagerstown silt loam soil (data points from *Jabro* [1996]). The solid line represents the
914 predictions of Equation (33), the dashed line shows the crack contribution to K_s and the dotted
915 line shows the aggregate contribution to K_s.

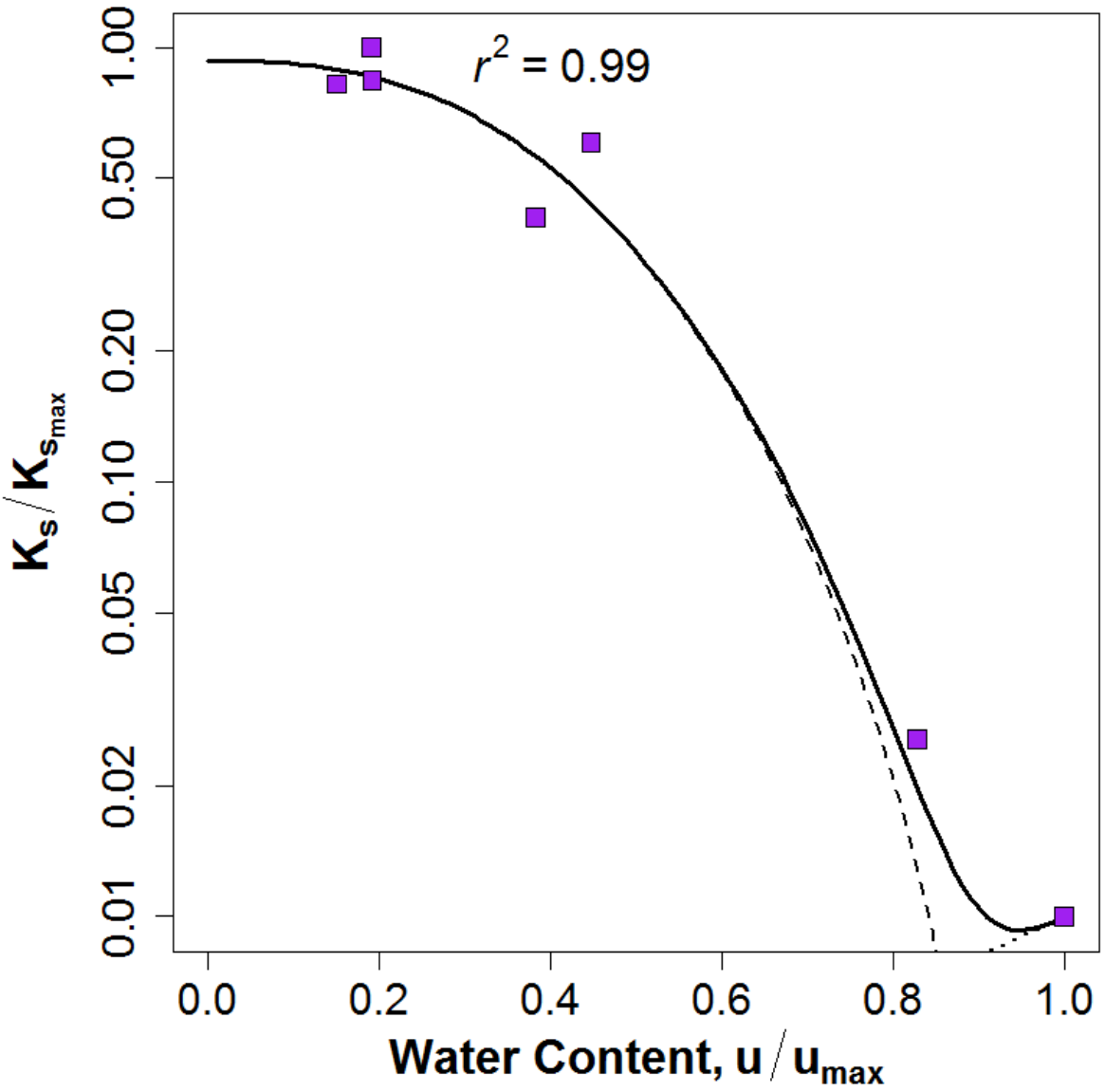

916

917 Figure 10 – Transient saturated hydraulic conductivity (K_s) versus water content (u/u_{max}) for a
918 Ships clay soil (Source: *Lin et al.* [1998]). Note that K_s values are scaled relative to the observed
919 maximum, based on steady-state infiltration rates. The solid line represents the predictions of
920 Equation (33), the dashed line shows the crack contribution to K_s and the dotted line shows the
921 aggregate contribution to K_s.